

AD-A165 228

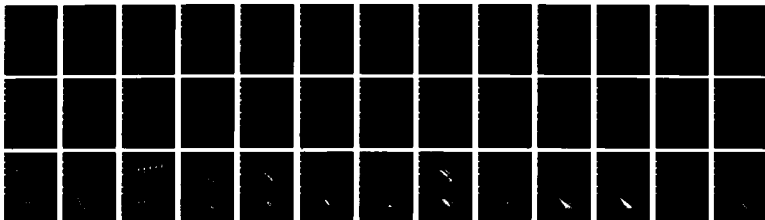
INVESTIGATION OF EURASIAN SEISMIC SOURCES AND UPPER
MANTLE STRUCTURE(U) MASSACHUSETTS INST OF TECH
CAMBRIDGE DEPT OF EARTH ATMOSPHERI T H JORDON

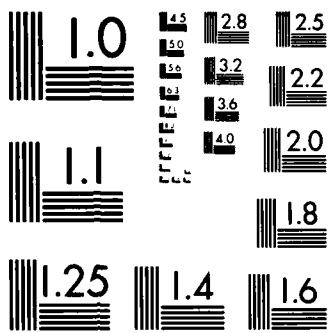
1/1

UNCLASSIFIED

30 JUN 85 AFGL-TR-85-0206 F19628-85-K-0024 F/G 8/11

NL





MICROCOPY RESOLUTION TEST CHART
NATIONAL BUREAU OF STANDARDS-1963-A

AFGL-TR-85-0206

Investigations of Eurasian Seismic Sources
and Upper Mantle Structure

Thomas H. Jordan

Massachusetts Institute of Technology
Dept of Earth, Atmospheric & Planetary Science
Cambridge, MA 02139

AD-A165 228

30 June 1985

Semi-Annual Report No. 1

APPROVED FOR PUBLIC RELEASE; DISTRIBUTION UNLIMITED

AIR FORCE GEOPHYSICS LABORATORY
AIR FORCE SYSTEMS COMMAND
UNITED STATES AIR FORCE
HANSCOM AIR FORCE BASE, MASSACHUSETTS 01731

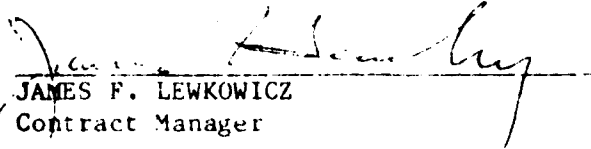
DTIC
E

DTIC FILE COPY

86 3 14 017

CONTRACTOR REPORTS

This technical report has been reviewed and is approved for publication.



JAMES F. LEWKOWICZ
Contract Manager



JAMES C. BATTIS
Acting Chief
Solid Earth Geophysics Branch

FOR THE COMMANDER



DONALD H. ECKHARDT
Director
Earth Sciences Division

This report has been reviewed by the ESD Public Affairs Office (PA) and is releasable to the National Technical Information Service (NTIS).

Qualified requesters may obtain additional copies from the Defense Technical Information Center. All others should apply to the National Technical Information Service.

If your address has changed, or if you wish to be removed from the mailing list, or if the addressee is no longer employed by your organization, please notify AFGL/DAA, Hanscom AFB, MA 01731. This will assist us in maintaining a current mailing list.

Unclassified

SECURITY CLASSIFICATION OF THIS PAGE

JD A165 225

REPORT DOCUMENTATION PAGE

1a. REPORT SECURITY CLASSIFICATION Unclassified		1b. RESTRICTIVE MARKINGS	
2a. SECURITY CLASSIFICATION AUTHORITY		3. DISTRIBUTION/AVAILABILITY OF REPORT Approved for public release; Distribution unlimited.	
2b. DECLASSIFICATION/DOWNGRADING SCHEDULE		4. PERFORMING ORGANIZATION REPORT NUMBER(S) 1	
4. PERFORMING ORGANIZATION REPORT NUMBER(S) 1		5. MONITORING ORGANIZATION REPORT NUMBER(S) AFGL-TR-85-0206	
6a. NAME OF PERFORMING ORGANIZATION Massachusetts Institute of Technology	6b. OFFICE SYMBOL	7a. NAME OF MONITORING ORGANIZATION Air Force Geophysics Laboratory	
6c. ADDRESS (City, State and ZIP Code) Dept of Earth, Atmospheric & Planetary Sci. Cambridge, MA 02139		7b. ADDRESS (City, State and ZIP Code) Hanscom Air Force Base, Massachusetts 01731	
8a. NAME OF FUNDING SPONSORING ORGANIZATION GARPA	8b. OFFICE SYMBOL (if applicable)	9. PROCUREMENT INSTRUMENT IDENTIFICATION NUMBER F19628-85-K-0024	
8c. ADDRESS (City, State and ZIP Code) 1400 Wilson Blvd. Arlington, VA 27709		10. SOURCE OF FUNDING NOS.	
11. TITLE (Include security classification) Investigations of Eurasian Seismic Sources and Upper Mantle Structure		PROGRAM ELEMENT NO. 61101F	PROJECT NO. 5A10
12. PERSONAL AUTHOR(S) Thomas H. Jordan		TASK NO. DA	WORK UNIT NO. AM
13a. TYPE OF REPORT Semi-annual #1	13b. TIME COVERED FROM 12/6/84 TO 6/30/85	14. DATE OF REPORT (Yr., Mo., Day) 1985 June 30	15. PAGE COUNT 38
16. SUPPLEMENTARY NOTATION			
17. COSATI CODES		18. SUBJECT TERMS (Continue on reverse if necessary and identify by block number)	
FIELD	GROUP	SUB GR	Eurasian structure; waveform inversion; higher-mode dispersion; resolving power
19. ABSTRACT (Continue on reverse if necessary and identify by block number) <i>and successfully fit</i>			
<p>(1) We have successfully fit complex P-SV wavegroups on vertical component seismograms for paths crossing northern Eurasia with a model having a 39-km crust and no asthenospheric low-velocity zone. Between the Moho and the 400-km discontinuity, the shear velocities found from the P-SV waveform analysis are consistently lower than those inferred from the SH waveform modeling of Grand and Helmberger. We suggest that this discrepancy is diagnostic of a polarization anisotropy associated with the olivine-rich mineralogy of the thick, basalt-depleted chemical boundary layer that characterizes the upper mantle beneath stable continents.</p> <p>(2) We investigate the vertical resolving power of source and receiver arrays in determining Eurasian crustal and upper mantle structure using the waveform inversion technique of Lerner-Lam and Jordan (1983). The results show that good resolution of upper mantle structure can be obtained with this method from sparse arrays of sources and/or receivers. Source arrays are particularly effective in enhancing resolution, provided that the source</p>			
20. DISTRIBUTION AVAILABILITY OF ABSTRACT UNCLASSIFIED UNLIMITED <input type="checkbox"/> SAME AS RPT <input checked="" type="checkbox"/> DTIC USERS <input type="checkbox"/>		21. ABSTRACT SECURITY CLASSIFICATION Unclassified	
22a. NAME OF RESPONSIBLE INDIVIDUAL James Lewkowicz		22b. TELEPHONE NUMBER (Include Area Code)	22c. OFFICE SYMBOL AFGL/LWH

Recovery of Eurasian Crustal and Upper-Mantle Structure by Higher-Mode Waveform Analysis

THOMAS H. JORDAN, ARTHUR L. LERNER-LAM*, AND LIND S. GEE

*Department of Earth, Atmospheric and Planetary Sciences
Massachusetts Institute of Technology, Cambridge, MA 02139*

This paper reviews the waveform inversion technique of *Lerner-Lam and Jordan* [1983] and reports on its application to the study of Eurasian crustal and upper-mantle structure. We have successfully fit complex P-SV wavegroups on vertical-component seismograms for paths crossing northern Eurasia with a model having a 39-km crust and no asthenospheric low-velocity zone. Between the Moho and the 400-km discontinuity, the shear velocities found from the P-SV waveform analysis are consistently lower than those inferred from the SH waveform modeling of *Grand and Helmberger*. We suggest that this discrepancy is diagnostic of a polarization anisotropy associated with the olivine-rich mineralogy of the thick, basalt-depleted chemical boundary layer that characterizes the upper mantle beneath stable continents, a hypothesis consistent with the higher-mode results of *Cara* and others. The algorithms employed in this study can be generalized to incorporate such anisotropic structures and can be applied to the construction of fully three-dimensional models of Eurasia, as well as to the study of upper-mantle attenuation structure.

INTRODUCTION

Seismological methods for the detection and discrimination of underground nuclear explosions rely on models of the crustal and upper-mantle structure, particularly attenuation structure in the vicinity of the testing areas. Estimates of the body-wave magnitude bias between the Eastern Kazakh Test Site, where the recent large Soviet shots have been fired, and the Nevada Test Site, which provides the bulk of the magnitude-yield calibration data, range from 0.2 to 0.4 magnitude units, corresponding to factors of about 1.6 to 2.8 in yield. The uncertainty in this bias dominates the errors in the yields determined from teleseismic P waves and has proven to be a source of controversy in verifying compliance with the Threshold Test Ban Treaty.

For fixed receiver networks, the body-wave attenuation bias is primarily controlled by local and regional variations in upper-mantle structure beneath the sources. These variations appear to be largest in the asthenosphere below 100 km. Recent models of the subcontinental mantle suggest that substantial variations in temperature and composition extend to depths exceeding 200 km and that these variations correlate with the long-term tectonic history of the overlying crust [*Jordan*, 1981]. Therefore, the problems of yield estimation are coupled to fundamental questions regarding continental evolution.

Previous work on mapping the three-dimensional structure of Eurasia has employed fundamental-mode surface waves [e.g., *Feng and Teng*, 1983], which lack sufficient resolution below 100-km depth, or a limited number of multiply reflected body waves with restricted geographical coverage [e.g., *Sipkin and Jordan*, 1976; *Burdick et al.*, 1983]. *Grand et al.* [1985] have recently extended the SS-S technique of *Burdick et al.* [1983] and *Grand and Helmberger* [1984] to include SSS phases and thereby increase the geographical range of the body-wave observations, but their work has thus far been confined to the forward modeling of SH-polarized signals.

* Now at Lamont-Doherty Geological Observatory, Palisades, NY 10964

In a DARPA/AFGL-sponsored project initiated this year, we are attempting to develop techniques for the systematic inversion of both P-SV and SH waveforms from higher-mode dispersed wave groups (which include multiply reflected body waves) for lateral heterogeneity. These methods are capable of giving much better vertical resolution of path-averaged properties than the dispersion of the fundamental-mode surface waves alone. They will be applied to large data sets collected from GDSN, NARS, WWSSN and other seismic networks to obtain three-dimensional models of Eurasian crustal and upper-mantle structure. Here we describe the formulation of the waveform inversion procedure and give the results of some preliminary modeling of the structure along paths traversing the northern part of Eurasia.

FORMULATION OF THE WAVEFORM-INVERSION TECHNIQUE

Our formulation is based on the mode-isolation and waveform-inversion techniques described by *Lerner-Lam and Jordan* [1983]. The observed seismogram is represented as the sum of fundamental ($n = 0$) and higher-mode ($n \geq 1$) surface waves:

$$s(t) = \sum_{n=0}^N u_n(t)$$

$u_n(t)$ is the seismogram for the n^{th} mode branch. A synthetic seismogram $\bar{s}(t)$ is calculated for a chosen, spherically symmetric earth model $m(r)$, and the difference between the observed and the synthetic is formed:

$$\Delta s(t) \equiv s(t) - \bar{s}(t) = \sum_{n=0}^N \Delta u_n(t)$$

$\Delta u_n(t)$ is the differential seismogram for the n^{th} mode branch.

To increase the signal-to-noise ratio (SNR) for a specified mode and reduce the interference from spurious signals and other modes, we construct matched filters from the synthetic branch seismograms. At the lag time τ we define the observed branch cross-correlation function (BCCF)

$$S_m(\tau) = \bar{u}_m(t) * s(t) = \int_{-\infty}^{\infty} \bar{u}_m(t) s(t + \tau) dt$$

and the synthetic BCCF

$$\bar{S}_m(\tau) = \bar{u}_m(t) * \bar{s}(t)$$

provides an approximate description of the mode-mode interference, so an appropriate data functional for the structural inverse problem is the differential BCCF,

$$\Delta S_m(\tau) = S_m(\tau) - \bar{S}_m(\tau) = \bar{u}_m(t) * \sum_{n=0}^N \Delta u_n(t)$$

In our procedure, we seek a model perturbation which to first order minimizes a quadratic form in ΔS_n . The quadratic form includes a symmetric taper about zero lag, so the points near $\tau = 0$, where the SNR is greatest, receive the most weight.

For the first-order, vertical-component surface waves received at stations far away from the source and its antipode, branch seismograms can be approximated by an integral over continuous wavenumber λ , whose asymptotic form is

$$u_n(\Delta, t) = \int_0^{\infty} G_n(\lambda, \Delta, t) \cos \xi_n(\lambda, \Delta, t) d\lambda$$

Δ is epicentral distance, and G_n and ξ_n are the amplitude and phase kernels

$$G_n(\lambda, \Delta, t) = \frac{|U_n| E_n}{2\pi (\sin\Delta)^{1/2}} \exp[-\alpha_n(\lambda) t]$$

$$\xi_n(\lambda, \Delta, t) = \lambda\Delta - \pi/4 - \omega_n(\lambda)t + \Phi_n$$

U_n and E_n are displacement and excitation scalars, Φ_n is the source phase, ω_n is the dispersion function, and $\alpha_n = \omega_n/2Q_n$ is the decay function. E_n and Φ_n depend on the source mechanism, whereas ω_n and α_n depend on the path-averaged elastic and anelastic parameters, respectively. The horizontal-component seismograms have similar forms.

We have developed an efficient algorithm for computing branch synthetics which is based on Filon quadrature. The algorithm is adaptive and reduces computation time by an order of magnitude over conventional mode-summation techniques [Lerner-Lam and Jordan, 1983].

Departures of the real earth from the spherically symmetric reference model m are represented as perturbations to the amplitude and phase kernels:

$$G_n(\lambda, \Delta, t) = \bar{G}_n(\lambda, \Delta, t) [1 + \gamma_n(\lambda)]$$

$$\xi_n(\lambda, \Delta, t) = \bar{\xi}_n(\lambda, \Delta, t) - \Delta\omega_n(\lambda) t$$

Here $\gamma_n(\lambda)$ is the perturbation to the relative amplitude of the n^{th} mode, and $\Delta\omega_n = \omega_n - \bar{\omega}_n$ is the perturbation to its dispersion function. If the perturbations to the displacement scalar U_n and the excitation scalar E_n can be ignored, a good approximation when the lateral variations along the path are small, then the relative amplitude perturbation can be written

$$\gamma_n(\lambda) = -\Delta\alpha_n(\lambda)t$$

where $\Delta\alpha_n = \alpha_n - \bar{\alpha}_n$, which in turn can be related to the perturbation in the specific attenuation

$Q_n^{-1}(\lambda)$. In terms of the differential BCCF, the linearized forward problem becomes

$$\Delta S_m(\tau) = \sum_{n=0}^N \int_0^{\infty} [B_{mn}(\lambda, \tau) \Delta \omega_n(\lambda) + D_{mn}(\lambda, \tau) \Delta \alpha_n(\lambda)] d\lambda$$

The partial derivatives B_{mn} and D_{mn} can be evaluated by the same adaptive Filon algorithm used to compute the synthetic seismograms. The integrals over wave-number are thereby discretized on the Filon grids $\{\lambda_{\ell}: \ell = 1, 2, \dots, L_n\}$. To set up a matrix system describing the differential BCCFs for $M+1$ mode branches ($m = 0, 1, \dots, M \leq N$) at each of P stations ($p = 1, 2, \dots, P$), we discretize the cross-correlations at the set of lag times $\{\tau_k = k \Delta \tau: k = -K, -K+1, \dots, 0, \dots, K-1, K\}$ and define the vectors

$$[\Delta S]_{mpk} = \Delta S_{mp}(\tau_k)$$

$$[\Delta \omega]_{n\ell} = \Delta \omega_n(\lambda_{\ell})$$

$$[\Delta \alpha]_{n\ell} = \Delta \alpha_n(\lambda_{\ell})$$

and the matrices

$$[B]_{mpk, n\ell} = B_{mnp}(\lambda_{\ell}, \tau_k)$$

$$[D]_{mpk, n\ell} = D_{mnp}(\lambda_{\ell}, \tau_k)$$

This yields the linearized, discretized forward problem

$$\Delta S = B \Delta \omega + D \Delta \alpha \quad (1)$$

The matrices appearing in this linear system have $I = (M+1) - P - (2K+1)$ rows and

$$J = \sum_{n=0}^N L_n$$

columns. For typical ranges of indices used in our work to date, these dimensions are on the order of 10^4 and 10^2 , respectively.

The vector ΔS can be computed from a set of observed seismograms, and equation (1) inverted for the perturbations to the dispersion and the attenuation functions. In practice, it is convenient to parameterize the vectors $\Delta \omega$ and $\Delta \alpha$ by perturbations Δm to the radial starting model. This reduces the dimension of the system and constrains the perturbed seismograms to correspond to a realistic earth structure. We interpret the resulting one-dimensional model as the average of the three-dimensional structure along the path between the source and receiver. Inversion procedures based on this representation have been discussed by *Lerner-Lam and Jordan* [1983].

APPLICATION TO EURASIAN DATA

The mode-isolation and waveform-inversion technique has been applied to seismograms recorded at five WWSSN stations in western Europe from four earthquakes in the Kuril-Kamchatka Seismic Zone (Figure 1). The focal depths for the events range from 134 km to 544 km, and the epicentral distances from 55° to 78° . The data set comprises a total of fourteen paths traversing a variety of tectonic structures in northern Eurasia, from the tectonically active region east of the Verkhoyansk Suture Zone to the Baltic Shield. The long-period, vertical-component seismograms were digitized, response-normalized, and low-pass filtered with a corner at 35 mHz.

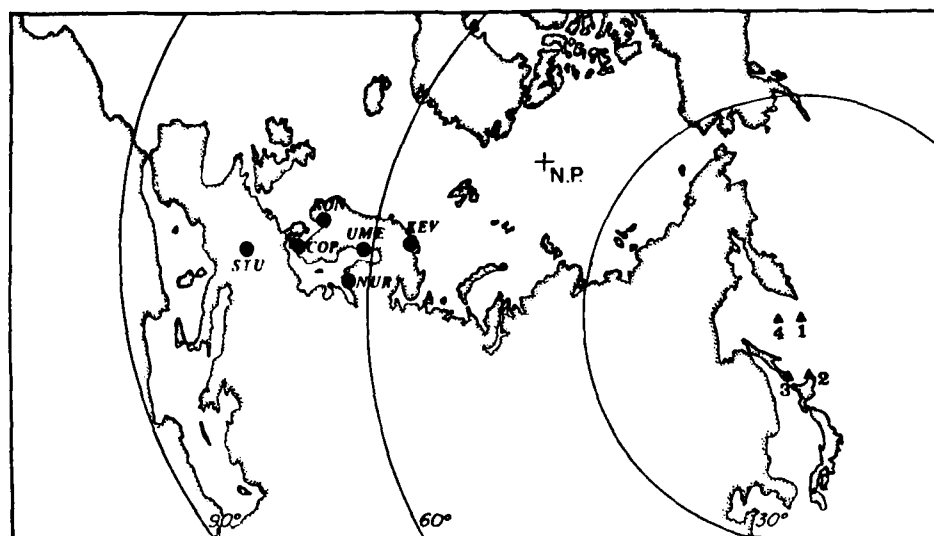


Figure 1. Azimuthal equidistant projection of the event-station distribution for the northern Eurasian path, with the pole centered on the epicenter of Event 1. The events, shown as triangles, range in focal depth from 134 to 544 km. The stations are shown as circles.

In our original analysis of this data set [Lerner-Lam and Jordan, 1983], we chose the very smooth structure of *Cara et al.* [1980] as a starting model and solved for shear-velocity perturbations that were a smooth function of depth. The modeling presented in this report is based on a layered structure with four upper-mantle discontinuities below the crust-mantle boundary and polynomial variations in the seismic velocities and density of each layer; the polynomials were taken to be linear throughout the upper mantle. Perturbations were allowed in the depths of all discontinuities, as well as in the parameters of the polynomials. The starting model was set equal to PREM [Dziewonski and Anderson, 1983] in the lower mantle and conformed to regionalized body-wave and surface-wave models of continental structure above this depth; it contained no low velocity zone.

The attenuation model used in our calculations was that of *Masters and Gilbert* [1983]. In these preliminary experiments, we did not attempt to invert for attenuation structure. We did, however, desensitize the inversion to possible amplitude fluctuations associated with Q variations and source effects using the normalization scheme described by *Lerner-Lam and Jordan* [1983, sect. 5.2], which employs a projection operator to annihilate the second term on the right-hand side of equation (1) for a restricted class of amplitude perturbations.

The model obtained from waveform inversion, EU2, is plotted in Figure 2. Comparisons of observed and synthetic waveforms and BCCFs are displayed in Figures 3-6. The structure is a simple one, but it provides a remarkably good fit to the phase of the waveforms over the entire range

of focal depths, including both the fundamental Rayleigh mode and the complex wave groups representing the interference of the higher modes. The pulses seen on the seismograms in Figure 6, for example, where the match is nearly wiggle-for-wiggle, are dominated by contributions from the third and fourth overtones. These waveforms can also be represented as the sum of multiply reflected P-SV body phases, predominantly SS and SSS; the agreement shows that the model satisfies their travel times. Our waveform analysis is thus the P-SV equivalent of the SH analysis performed by *Grand and Helmberger [1984a,b]*, and our resolution of sub-lithospheric structure should be comparable to theirs. (Because our technique is formulated as a linearized inverse problem, its resolving power can be analyzed using formal linear methods, which is one of its major advantages over forward-modeling. Preliminary calculations have been made by *Lerner-Lam [1983]*, and a more detailed resolving-power study is given by *Gee et al. [1985]*.)

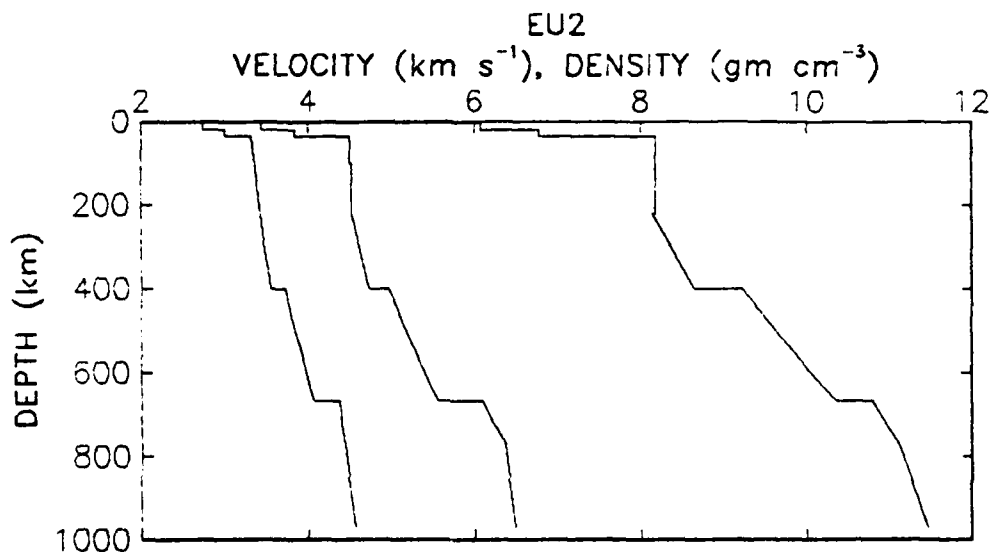
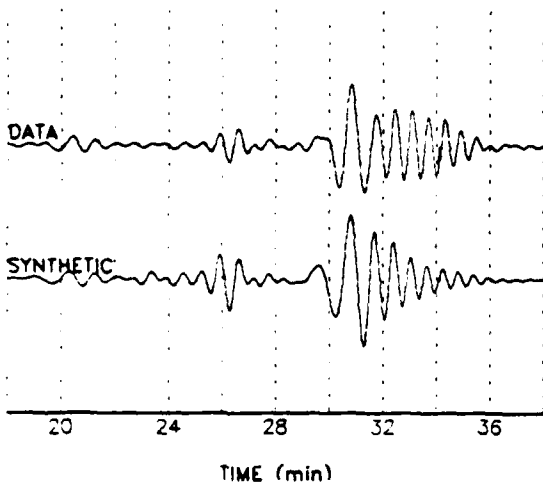


Figure 2. EU2, a path-averaged model of northern Eurasia obtained by waveform inversion of fundamental and higher-mode surface waves.

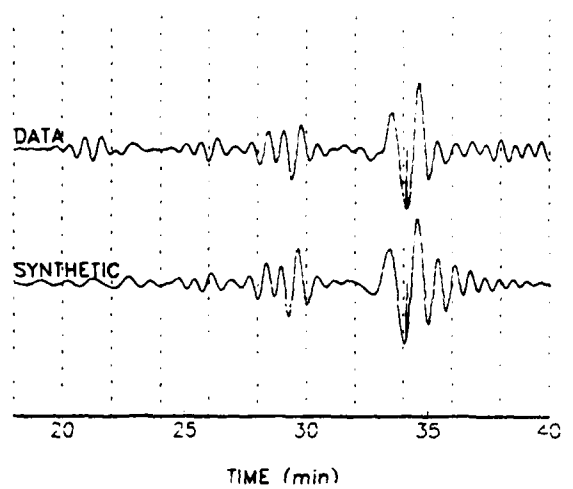
EU2 shear velocities are compared with the SNA model of *Grand and Helmberger [1984a]* in Figure 7. The latter structure was derived from S and SS waves traversing the Canadian Shield, but *Grand et al. [1985]* have shown that it also provides a good description of SH propagation across the stable platforms of Eurasia. The two models have comparable velocity jumps at 400 km and are in good agreement below this depth. However, above 400 km, there are significant differences between the two structures. SNA has a low-velocity zone centered at about 200-km depth, whereas the shear velocities in EU2 increase monotonically throughout the upper mantle. Experiments with this and other parameterizations, including structures parameterized by continuous variations with depth, indicate that our data set cannot be satisfied by a model with an LVZ as pronounced as SNA; the velocity variation between 100 km and 200 km is tightly constrained by the difference in the arrival times of the fundamental and first higher-mode wave groups, which are well observed on many of the seismograms used in this study.

The most obvious discrepancy between the two models is the negative offset in the shear velocity of EU2 relative to SNA throughout the mantle above 400 km, which averages 0.16 km/s. The differences are largest in the uppermost mantle (the lid of SNA), where they locally reach 0.27 km/s, but remain substantial even below 200 km. Given the high resolution of both methods in the interval 200-400 km, the differences appear to be real. For example, inversions of our data set with

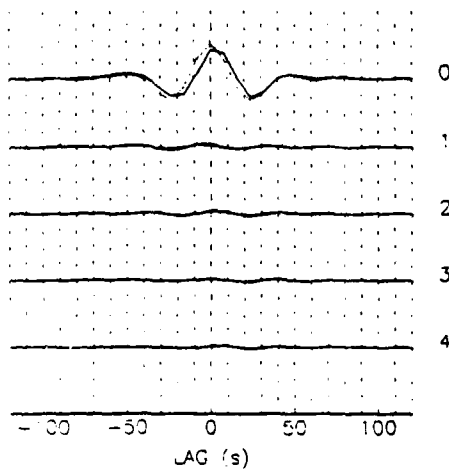
EVENT 1 NUR



EVENT 2 KON



EVENT 1 NUR



EVENT 2 KON

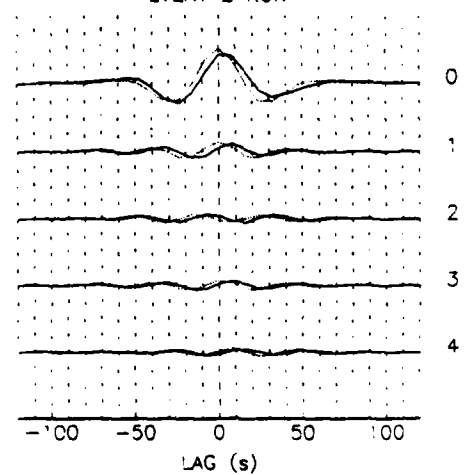
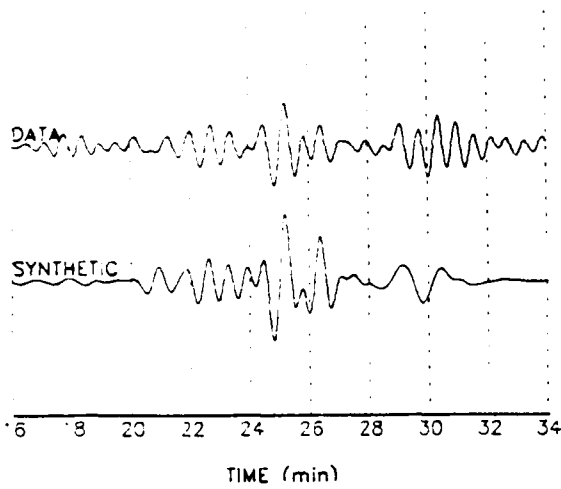


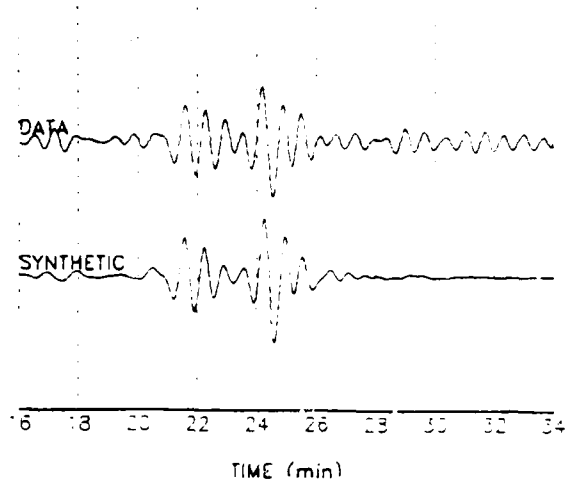
Figure 3. Comparisons of observed and synthetic waveforms (top panel) and BCCFs (bottom panel) recorded at NUR for Event 1 ($h = 134$ km). BCCFs plotted as solid lines observed, those plotted as dotted traces are synthetic. The BCCF mode number is to the right of each pair of traces in the lower panel. The energy in the waveforms is concentrated in the fundamental mode, which appears as the well-dispersed wavetrain beginning at about 29 min, although the S and SS arrivals are also visible at 20 min and 25 min.

Figure 4. Comparisons of observed and synthetic waveforms and BCCFs for Event 2 ($h = 181$ km) recorded at KON. Increased relative amplitude levels of the higher-modes are due to the increase in source depth.

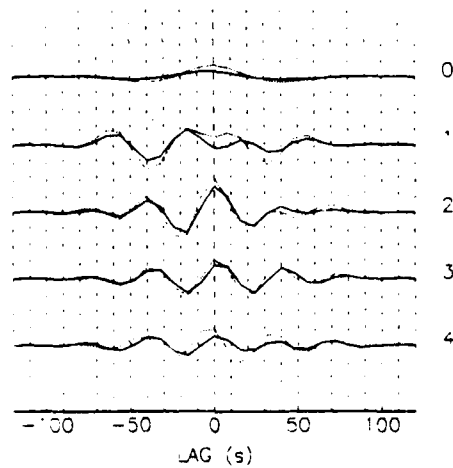
EVENT 3 UME



EVENT 4 NUR



EVENT 3 UME



EVENT 4 NUR

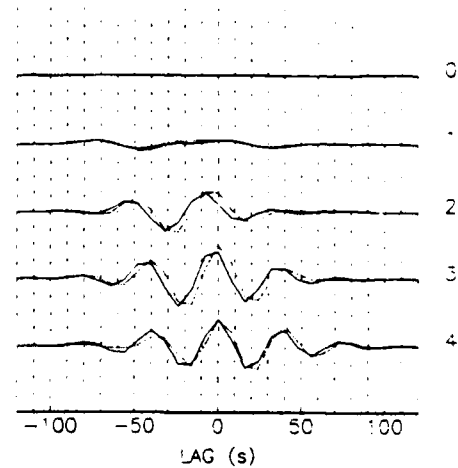


Figure 5. Comparisons of observed and synthetic waveforms and BCCFs for Event 3 ($h = 344$ km) recorded at UME. Fundamental mode energy is still visible at 29 minutes, but the record is dominated by higher-mode arrivals.

Figure 6. Comparisons of observed and synthetic waveforms and BCCFs for Event 4 ($h = 544$ km) recorded at NUR. Fundamental mode energy is almost totally absent from the waveforms; complex higher-mode arrivals dominate the signal. Near wiggle-for-wiggle fits are seen for the second, third, and fourth higher modes.

the velocities in this layer constrained at SNA values yield very poor fits to the observed seismograms.

Some of the discrepancy may result from the lower velocities encountered along the portions of the surface-wave paths traversing the tectonically active areas of northeastern Asia, but we are skeptical that an explanation based on path differences can account for it entirely. *Grand et al. [1985]* have modeled the transition from the active foldbelts of central Asia to the Russian platform using their multiple-S technique, and the *lowest* average velocities they find are still higher than those of EU2, even though the latter is derived from a data set primarily sampling the high-velocity shields and platforms of northern Eurasia.

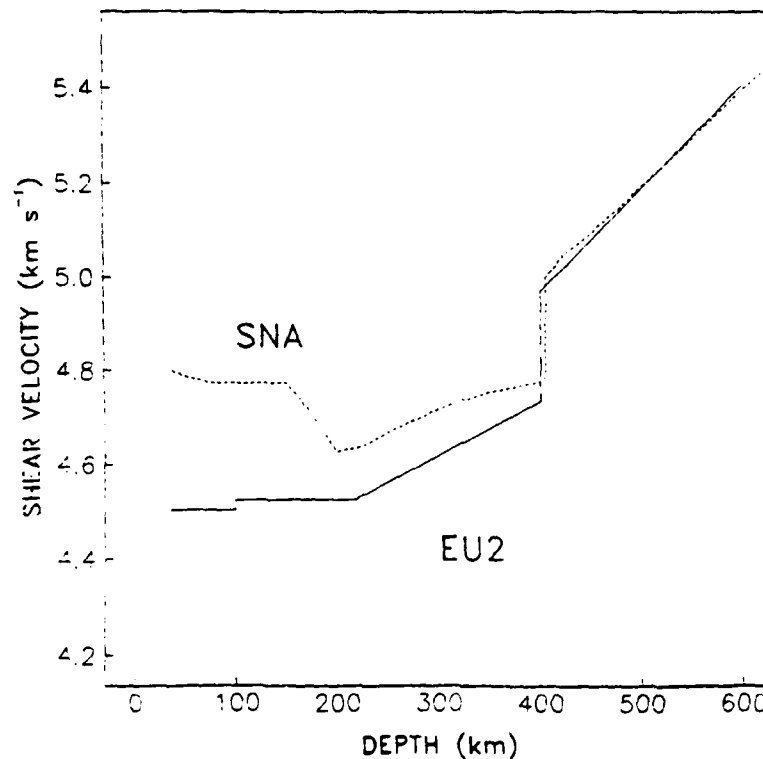


Figure 7. Comparison of EU2 shear velocities (solid line) with model SNA (dotted line) of *Grand and HelMBERGER (1984a)*. SNA was derived from SH-polarized S and SS waves traversing the Canadian Shield, but is representative of SH propagation across stable Eurasian platforms (*Grand et al. 1985*). EU2, derived from vertical-component higher-mode surface waves, is representative of P-SV propagation. The structures are virtually identical below the 400 km discontinuity, but exhibit distinct velocity differences in the upper mantle above 400 km.

Although a definitive statement must await the treatment of both P-SV and SH data sets from common paths by the same inversion technique (which is one of our goals for the next year), we suspect that the discrepancy in the average shear velocity between EU2 and SNA is diagnostic of deep-seated polarization anisotropy in the Eurasian upper mantle. This hypothesis is consistent with the observations and modeling results of *Cara et al. [1980]*, who found similar differences in SV and SH velocities from the inversion of higher-mode Rayleigh and Love waves. We speculate that this anisotropy is associated with the existence of a thick, basalt-depleted (and therefore olivine-rich) chemical boundary layer beneath Eurasia [*Jordan, 1981*].

FUTURE WORK

The waveform-inversion technique described in this report will be extended to include polarization anisotropy and variations in attenuation structure. We will apply the method to three-component data collected from GDSN, NARS, WWSSN and other seismic networks to obtain models of the crust and upper mantle over various Eurasian paths. These models will be employed to constrain the three-dimensional structure of the Eurasian continent.

Acknowledgement. This research was sponsored by the Defense Advanced Research Projects Agency and the Air Force Geophysical Laboratory under contract F19628-85-K-0024.

REFERENCES

- Burdick, L.J., S. Grand, D.V. Helmberger, T. Lay, and J. Rial, *Remote Sensing of Attenuation Bias using SS*, Report WCCP-R-83-01, Woodward-Clyde Consultants, Pasadena, 158 pp., 1983.
- Cara, M., A. Nercessian, and G. Nolet, New inferences from higher mode data in western Europe and northern Eurasia, *Geophys. J. R. Astr. Soc.*, **61**, 459-478, 1980.
- Dziewonski, A.M., and D.L. Anderson, Preliminary reference earth model, *Phys. Earth Planet. Inter.*, **25**, 297-356, 1981.
- Feng, C.-C., and T.-L. Teng, Three-dimensional crust and upper mantle structure of the Eurasian continent, *J. Geophys. Res.*, **88**, 2261-2272, 1983.
- Gee, L.S., A.L. Lerner-Lam, and T.H. Jordan, Resolving power of higher-mode waveform inversion for Eurasian upper-mantle structure, this report, 1985.
- Grand, S.P., and D.V. Helmberger, Upper mantle shear structure of North America, *Geophys. J. R. Astr. Soc.*, **76**, 399-438, 1984 a.
- Grand, S.P., and D.V. Helmberger, Upper mantle shear structure beneath the northwest Atlantic Ocean, *J. Geophys. Res.*, **89**, 11465-11475, 1984 b.
- Grand, S.P., D.V. Helmberger, and L.J. Burdick, *Attenuation Bias Measurements of the Semipalatinsk and North African Test Sites from Multiple S Phases*, Report WCCP-R-85-01, Woodward-Clyde Consultants, Pasadena, 27 pp., 1985.
- Jordan, T.H., Continents as a chemical boundary layer, *Phil. Trans. R. Soc. London, Ser. A*, **301**, 359-373, 1981.
- Lerner-Lam, A.L., and T.H. Jordan, Earth structure from fundamental and higher-mode waveform analysis, *Geophys. J. R. Astr. Soc.*, **75**, 759-797, 1983.
- Masters, G., and F. Gilbert, Attenuation in the earth at low frequencies, *Phil. Trans. R. Soc. London, Ser. A*, **308**, 479-522, 1983.
- Sipkin, S.A., and T.H. Jordan, Lateral heterogeneity in the upper mantle determined from the travel times of multiple ScS, *J. Geophys. Res.*, **81**, 6307-6320, 1976.

Resolving Power of Higher-Mode Waveform Inversion for Eurasian Upper-Mantle Structure

LIND S. GEE, ARTHUR L. LERNER-LAM*, AND THOMAS H. JORDAN

*Department of Earth, Atmospheric and Planetary Sciences
Massachusetts Institute of Technology, Cambridge, MA 02139*

In three-dimensional studies of earth structure based on surface-wave tomography, horizontal resolution is limited primarily by the distribution of paths, while vertical resolution is governed by the distribution of mode types. To obtain good vertical resolution below 200-km depth requires the use of higher modes. This paper investigates the vertical resolving power of source and receiver arrays in determining Eurasian crustal and upper-mantle structure using the waveform inversion technique of *Lerner-Lam and Jordan* [1983]. Unlike approaches to higher-mode analysis which rely on stacking to separate modes in the frequency-wavenumber domain, this procedure isolates the modes in the time domain by cross correlating a mode-branch synthetic with the observed and synthetic seismograms. The difference between the observed and synthetic branch cross-correlation functions is approximated as a linear functional of the residual dispersion, which is parameterized in turn by perturbations to earth structure. These differential branch cross-correlation functions are inverted for model perturbations, from which new dispersion curves and synthetic seismograms are computed, and the process is iterated until convergence. This formulation permits evaluation of real and hypothetical data sets by the resolution and covariance analysis of solutions to the linearized inverse problem. The results show that good vertical resolution of upper-mantle structure can be obtained with this method from sparse arrays of sources and/or receivers. Source arrays are particularly effective in enhancing resolution, provided that the source depths are well distributed and the source centroids and moment tensors are well determined. Resolution at depth may be obtained with this technique even with shallow sources, as long as the higher-mode branch cross-correlation functions are weighted appropriately.

INTRODUCTION

Studies of multiply-reflected shear waves, such as ScS_n [*Sipkin and Jordan*, 1976] and SS [*Grand et al.*, 1985], as well as studies of Rayleigh-wave dispersion [*Feng and Teng*, 1983], indicate that there are substantial lateral variations in upper-mantle structure underlying the Eurasian continent to depths exceeding 200 km. Recent models of the composition and development of the subcontinental mantle [*Jordan*, 1978, 1981; *Davies*, 1979; *Richter*, 1985] attribute this heterogeneity to compositional and thermal differences associated with the structure of what *Jordan* [1975] has termed the 'continental tectosphere.' These models predict a strong correlation between surface geological features and upper-mantle heterogeneity, a hypothesis which may be tested by detailed seismic imaging of the Eurasian crust and upper mantle.

One approach to such three-dimensional studies in Eurasia employs fundamental-mode Rayleigh waves to constrain lateral variations in structure [*Feng and Teng*, 1983]. While good horizontal resolution is possible with this technique, fundamental-mode dispersion is not sensitive to details in vertical structure at depths greater than 200 km. In principle, the addition of higher-mode data can improve structural resolution, but mode-mode interference complicates the

* Now at Lamont-Doherty Geological Observatory, Palisades, NY 10964

measurement of dispersion in both the time and frequency domain [Cara, 1978; Lerner-Lam, 1982]. One method of analysis of higher-mode information requires sophisticated processing of the data in the frequency-wavenumber domain to separate the modes [Nolet, 1975, 1976; Cara, 1978, 1979; Chou and Dziewonski, 1980]. While this technique has been used successfully in studies of one-dimensional structure in Eurasia [Nolet, 1975; Cara et al., 1980; Chou and Dziewonski, 1981], the Pacific [Cara, 1979], and North America [Cara, 1978, 1979], the procedure requires an array of stations distributed over several thousand kilometers and more-or-less aligned along the path from the epicenter. This requirement restricts the number of paths which may be studied with existing seismic networks and therefore limits the applicability of the method to tomographic experiments.

A different approach to higher-mode analysis has been taken by Lerner-Lam and Jordan [1983]. They employ waveform inversion to model the difference between an observed and synthetic seismogram as a measure of the departure of an earth model from an average of structure along the path. These differential seismograms are parameterized by perturbations to the fundamental and higher-mode dispersion, which are related to perturbations to the earth model. In traditional waveform inversion methods, the differential seismograms are inverted directly for model perturbations, with some weighting scheme applied on a time point by time point basis. However, Lerner-Lam and Jordan [1983] isolate higher-mode information explicitly by cross correlating the differential seismograms with the mode-branch synthetics and windowing the result in the lag-time domain. In addition to enhancing the signal-to-noise ratio for a particular mode and reducing interference from spurious signals and other modes, this approach permits the contribution from each mode to be assessed and weighted individually. The forward problem relating the branch cross-correlation functions to model perturbations is linearized by the application of first-order perturbation theory. Solutions are derived by a generalized least-squares inverse, and the process is iterated to convergence. The information provided by this approach is equivalent to the waveform analysis of multiply-reflected body waves [Grand and Helmberger, 1984a,b; Grand et al., 1985], which uses trial-and-error forward modelling techniques. However, the ability of these methods to resolve upper-mantle structure is difficult to assess, whereas the linearized formulation used in this study permits the evaluation of the solutions by the now standard resolving power analysis of linear inverse theory.

In the next few years, millions of dollars will be spent on the deployment of new digital seismic instruments around the world. In particular, the Incorporated Research Institutes for Seismology (IRIS) network and the Portable Array of Seismometers for Studies of the Crust and Lithosphere (PASSCAL) will be coming on-line in the near future. In order to maximize the benefit from this expansion, it is important to understand how various configurations of sources and receivers will affect the resolution of earth structure. For example, an array of seismometers recently has been established in Western Europe. The Network of Autonomously Registering Stations (NARS) array spans 2500 km with 14 receivers [Nolet, Dost, and Paulssen, 1984]. One question which needs to be addressed is whether dense, linear arrays such as NARS are essential for detailed studies of upper-mantle structure. While the higher-mode wavenumber-stacking techniques of Nolet [1975, 1976] and Cara [1978, 1979] require this type of array to obtain the necessary spatial coverage, the waveform inversion technique of Lerner-Lam and Jordan [1983], which makes use of *a priori* information about structure along the path, does not. Consequently, a more efficient deployment of such receiver arrays would distribute them over a larger area in order to sample the greatest number of source-receiver paths.

FORMULATION OF THE INVERSE PROBLEM

In the waveform inversion technique of Lerner-Lam and Jordan [1983], an observed seismogram is characterized as the sum of the fundamental ($n = 0$) and higher-mode ($n \geq 0$)

surface waves:

$$s(\mathbf{r}, t) = \sum_{n=0}^{\infty} u_n(\mathbf{r}, t) \quad (1)$$

where $u_n(\mathbf{r}, t)$ is the seismogram for the n^{th} mode branch at a receiver position \mathbf{r} and time t . A synthetic seismogram, $s(\mathbf{r}, t)$, is calculated for a particular spherically-symmetric earth model, $m(r)$, complete to radial order N :

$$\bar{s}(\mathbf{r}, t) = \sum_{n=0}^N \bar{u}_n(\mathbf{r}, t) \quad (2)$$

where $\bar{u}_n(\mathbf{r}, t)$ is the synthetic seismogram for the n^{th} mode branch. In our application of this technique, the sum over N is truncated at the seventh higher mode (Figure 1). Although phases of high apparent velocity, such as core reflections, are not well represented as a consequence, these phases are nearly transversely polarized and do not contribute to the vertical-component seismograms used in this study. $u_n(\mathbf{r}, t)$ is formulated using an asymptotic approximation to Gilbert's [1976] exact travelling-wave representation of the displacement field:

$$\bar{u}_n(\mathbf{r}, t) \sim \sum_{s=1}^S \int_0^{\infty} \bar{G}_n^s(\lambda, \mathbf{r}, t) \cos \bar{\xi}_n^s(\lambda, \mathbf{r}, t) d\lambda. \quad (3)$$

In this formulation, λ is the surface spherical wavenumber, and $\bar{G}_n^s(\lambda, \mathbf{r}, t)$ and $\bar{\xi}_n^s(\lambda, \mathbf{r}, t)$ are the amplitude and phase kernels for the s^{th} orbit of the n^{th} higher mode. Since we are concerned with arrivals corresponding to the first (minor-arc) orbit, we take $s = 1$ and drop the orbital indices.

The difference between an observed and synthetic seismogram, $\Delta s(\mathbf{r}, t)$, can be approximated as a radial perturbation, $\Delta m(r)$, to the starting earth model, $m(r)$, where

$$\Delta s(\mathbf{r}, t) = s(\mathbf{r}, t) - \bar{s}(\mathbf{r}, t) = \sum_{n=0}^N \Delta u_n(\mathbf{r}, t) \quad (4)$$

and $\Delta u_n(\mathbf{r}, t)$ is the differential seismogram for the n^{th} mode branch. In order to estimate $\Delta m(r)$ from $\Delta s(\mathbf{r}, t)$, it is necessary to minimize both observational and representational errors. These include random seismic noise and digitizing errors, as well as error processes which scale with signal strength, such as inaccuracies in representing the source, the instrument response, and wave propagation through the earth. One method of enhancing the signal corresponding to a particular mode and reducing the effect of ambient noise and spurious signals is to construct matched filters [Chou and Dziewonski, 1980] by cross correlating the differential seismograms with the mode-branch synthetics and windowing the results in the lag-time domain. Lerner-Lam and Jordan [1983] define the observed branch cross-correlation function,

$$S_m(\mathbf{r}, \tau) = \bar{u}_m(\mathbf{r}, t) * s(\mathbf{r}, t) \equiv \int_{-\infty}^{\infty} \bar{u}_m(\mathbf{r}, t) s(\mathbf{r}, t + \tau) dt \quad (5)$$

and the synthetic branch cross-correlation function,

$$\bar{S}_m(\mathbf{r}, \tau) = \bar{u}_m(\mathbf{r}, t) * \bar{s}(\mathbf{r}, t) \quad (6)$$

where τ is the lag time. With this notation, an appropriate functional for the structural inverse problem is the differential branch cross-correlation function:

$$\Delta S_m(\mathbf{r}, \tau) = S_m(\mathbf{r}, \tau) - \bar{S}_m(\mathbf{r}, \tau) \cong \bar{u}_m(\mathbf{r}, t) * \sum_{n=0}^N \Delta u_n(\mathbf{r}, t) \quad (7)$$

Using first-order perturbation theory, $\Delta S_m(\mathbf{r}, \tau)$ may be related linearly to amplitude and dispersion perturbations through variations to the amplitude and phase kernels of $u_n(\mathbf{r}, t)$

$$G_n(\lambda, \mathbf{r}, t) = \bar{G}_n(\lambda, \mathbf{r}, t) [1 + \gamma_n(\lambda)] \quad (8a)$$

$$\xi_n(\lambda, \mathbf{r}, t) = \bar{\xi}_n(\lambda, \mathbf{r}, t) - \Delta\omega_n(\lambda)t \quad (8b)$$

where $\gamma_n(\lambda)$ is a wavenumber-dependent perturbation to the relative amplitude and $\Delta\omega_n = \omega_n - \bar{\omega}_n$ is a perturbation to the dispersion of the n^{th} higher mode. In terms of the differential branch cross-correlation function,

$$\Delta S_m(\mathbf{r}, \tau) \cong \sum_n \int_0^\infty [C_{mn}(\lambda, \mathbf{r}, \tau) \gamma_n(\lambda) + B_{mn}(\lambda, \mathbf{r}, \tau) \Delta\omega_n(\lambda)] d\lambda \quad (9)$$

where $C_{mn}(\lambda, \mathbf{r}, \tau)$ and $B_{mn}(\lambda, \mathbf{r}, \tau)$ are the cross correlations of the mode-branch synthetics with the Fréchet kernels for the amplitude and dispersion perturbations. This linearization is valid, provided that

$$|\Delta\omega_n t| \ll 1 \quad (10a)$$

$$|\gamma_n| \ll 1. \quad (10b)$$

In general, these conditions will not be met, and the inversion must be iterated. Equation (9) can be rewritten in matrix form,

$$\Delta S = C\gamma + B\Delta\omega. \quad (11)$$

By applying Rayleigh's principle and first-order perturbation theory, the dispersion can be parameterized in terms of perturbations to the reference model [Woodhouse and Dahlen, 1978]:

$$\Delta\omega = H\Delta m \quad (12)$$

where H is the Fréchet kernel for the appropriate model parameter. The relationship between the amplitude perturbation and the model perturbation is more complicated, however, and depends on details of the source and path. *Lerner-Lam and Jordan* [1983] apply an orthogonalization procedure to reduce the sensitivity of the branch cross-correlation functions to amplitude differences between the observed and synthetic seismogram. Their approach utilizes a projection operator to annihilate the matrix C . In this study, we consider only perturbations to the dispersion and disregard perturbations to the amplitude kernel.

With this formulation, the linearized forward problem between the differential branch cross-correlation function, ΔS , and perturbations to the reference earth model, Δm , reduces to:

$$A \Delta m = \Delta S \quad (13)$$

where $A = BH$. So far we have not considered the effect of noise or errors in the data functionals. In general, the estimated differential branch cross-correlation function, ΔS_e , will be the sum of the true branch cross-correlation function, ΔS , and some error, n , such that:

$$\Delta S_e = \Delta S + n \quad (14)$$

We assume that the expected value of n is zero,

$$\langle n \rangle = 0 \quad (15)$$

and therefore its covariance matrix is

$$V_n = \langle nn^T \rangle \quad (16)$$

If the observational errors are uncorrelated, then V_n will be diagonal. This is almost never the case, but we will follow in the footsteps of many others and assume it to be true. At this point, there is not enough known about the error processes to model them in a more sophisticated way.

Rescaling equation 13 to account for the observational and representational errors:

$$\hat{A}\Delta m = \hat{\Delta S} + \hat{n} \quad (17)$$

where Δm is now a stochastic process whose mean satisfies equation 13 and

$$\hat{A} = V_n^{-1/2} A \quad (18a)$$

$$\hat{\Delta S} = V_n^{-1/2} \Delta S \quad (18b)$$

$$\hat{n} = V_n^{-1/2} n. \quad (18c)$$

With this scaling, \hat{n} is a zero-mean stochastic process whose covariance matrix is equal to the identity operator $\mathbf{1}$. In practice, we assume that the diagonal elements of $V_n^{-1/2}$ corresponding to the j^{th} lag-time point, t_j , of the i^{th} branch cross-correlation function are of the form $\sigma_i^{-1} W(t_j)$, where $W(t)$ is a cosine-square taper of width τ . Thus, σ_i is the standard deviation at zero lag.

Lerner-Lam and Jordan [1983] solve the linearized forward problem of equation 17 using generalized least-squares and imposing the conditions of regularization and smoothness:

$$\|\Delta \hat{S}_e - \hat{A} \Delta m\|^2 + \alpha \|\Delta m\|^2 + \beta \|D^2 \Delta m\|^2 = \min \quad (19)$$

where $\|\Delta \hat{S}_e - \hat{A} \Delta m\|^2$ is the least-squares measure of data misfit, $\|\Delta m\|^2$ is the model perturbation size, D^2 is the second difference operator, $\|D^2 \Delta m\|^2$ is the model perturbation smoothness, and α and β are the scalar trade-off parameters which control the weighting of one term relative to another. The regularization has the effect of reducing the contribution of the poorly-determined eigenvalues, while the smoothness constraint controls the oscillations of the solution about the starting model. Together, they stabilize the inversion. The solution to this minimization problem yields an estimate of the model perturbation, Δm

$$\Delta \tilde{m} = \hat{A}^\dagger \Delta \hat{S}_e \quad (20)$$

where \hat{A}^\dagger is an operator of the form:

$$\hat{A}^\dagger = (\hat{A}^T \hat{A} + \alpha \mathbf{I} + \beta D^{2T} D^2)^{-1} \hat{A}^T. \quad (21)$$

Equations 20 and 21 constitute the generalized least-squares solution to the forward problem posed by equation 17. This formulation of the waveform inversion technique is advantageous in that it isolates the modes in the time domain, obviating the need for complicated processing of the data in the frequency-wavenumber domain. In particular, this approach permits the contribution from each mode to be assessed and weighted individually. Extensive tests with synthetic data [*Lerner-Lam*, 1982] show that the linearization of equations 8a and b may break down when the starting model is sufficiently far from the true structure, locking the inversion into a spurious minimum. However, this condition may be identified readily by direct comparison of with the synthetic seismograms with the data and corrected by initializing the inversion with an appropriate perturbation to the starting model.

RESOLVING POWER ANALYSIS

Since the forward problem has been linearized by the application of first-order perturbation theory, its solutions for any particular data set may be evaluated with the full power of linear inverse theory. For example, we can compute the expected value of the estimated model perturbation:

$$\begin{aligned}
 \langle \Delta \tilde{\mathbf{m}} \rangle &= \langle \hat{\mathbf{A}}^\dagger \Delta \hat{\mathbf{S}} + \hat{\mathbf{A}}^\dagger \hat{\mathbf{n}} \rangle \\
 &= \langle \hat{\mathbf{A}}^\dagger \hat{\mathbf{A}} \Delta \mathbf{m} \rangle + \langle \hat{\mathbf{A}}^\dagger \hat{\mathbf{n}} \rangle \\
 &= \mathbf{R}_m \Delta \mathbf{m} .
 \end{aligned} \tag{22}$$

$\mathbf{R}_m = \hat{\mathbf{A}}^\dagger \hat{\mathbf{A}}$ is called the model resolution operator [Wiggins, 1972; Menke, 1984] and $\Delta \mathbf{m}$ is the exact model perturbation which satisfies equation 13. We can see from this analysis that \mathbf{R}_m acts as a filter on $\Delta \mathbf{m}$. If \mathbf{R}_m is the delta function which satisfies the constraint of unimodularity, then our estimate of the model perturbation will be exact. In general, \mathbf{R}_m is not a delta function and our estimate of $\Delta \mathbf{m}$ is a weighted average of the true model perturbation. A solution is considered to have 'good' resolution if the kernel is narrow and well localized; i.e. if it is peaked and has small sidelobes.

We can also calculate the covariance matrix of the model estimates, \mathbf{V}_m :

$$\begin{aligned}
 \mathbf{V}_m &= \langle (\Delta \tilde{\mathbf{m}} - \langle \Delta \tilde{\mathbf{m}} \rangle) (\Delta \tilde{\mathbf{m}} - \langle \Delta \tilde{\mathbf{m}} \rangle)^T \rangle \\
 &= \hat{\mathbf{A}}^\dagger \langle \hat{\mathbf{n}} \hat{\mathbf{n}}^T \rangle \hat{\mathbf{A}}^\dagger T \\
 &= \hat{\mathbf{A}}^\dagger \hat{\mathbf{A}}^\dagger T .
 \end{aligned} \tag{23}$$

\mathbf{V}_m characterizes the errors in the model estimates induced by errors in the data. The diagonal elements of the covariance operator represent the marginal variance of the model values, while the off-diagonal elements measure the correlation between the errors at one depth with the errors at other depths.

The properties of \mathbf{R}_m and \mathbf{V}_m depend on the earth model, the source and receiver geometry, and the weighting and windowing operators. There is a well-known trade-off between resolution and covariance [Backus and Gilbert, 1970], which is governed by the parameters α and β in this study. Varying α and β in a fixed ratio will translate the solution along a trade-off curve between the ability to resolve detail and the reliability of the estimate.

EXPERIMENTS

Although Lerner-Lam and Jordan [1983] recognized that their formulation permitted the

resolving power analysis by standard linear methods, they did not use it to assess their solutions. In this study, we incorporate the resolving power analysis into the waveform inversion technique and use this capability to examine some issues in experimental design. We approach this problem by designing a hypothetical array of five stations, located on the Baltic Shield and distributed over a distance of 1600 km (Table 1). This receiver distribution, which is similar to the configuration used in the study by *Lerner-Lam and Jordan* [1983], is modelled after the NARS array in order to examine the contribution of such dense, linear arrays to studies of upper-mantle structure. A cluster of five earthquakes which occurred in the two-year period 1982-1984 is selected as the source array (Table 2). Located south of Japan, these events range in depth from 119 to 552 km and have well-determined centroids and moment tensors from the Harvard solutions [*Dziewonski et al.*, 1981, 1983, 1984]. Vertical-component synthetic seismograms were calculated in the frequency band from 5 to 35 mHz using Lerner-Lam's asymptotic travelling-wave programs with *Cara et al.*'s [1980] model of Eurasian structure and the attenuation model of *Masters and Gilbert* [1983]. Figure 2 is a map of the source and receiver distribution considered in this study and Figure 3 is an example of the synthetic seismograms generated for this array for a shallow and deep event. The base station of this array, KONO01, coincides with the Global Digital Seismic Network station KONO. Only the fundamental and the first four higher-mode branch cross-correlation functions were included in the resolving power calculations.

With this configuration of sources and receivers, we explore the shear-wave velocity resolving power of the higher-mode waveform inversion technique. In particular, we consider four end-member cases: a single source recorded at one and five receivers and five sources recorded at one and five receivers. We also examine the influence of errors in the data by experimenting with the relative weighting of the branch cross-correlation functions. In the first six experiments, we model the errors as stochastic processes by weighting the branch cross-correlation functions equally. This 'natural' weighting allows the mode branch with the highest amplitude (and consequently the highest signal-to-noise ratio) to control the inversion. In the last two experiments, we model the errors as processes which scale with signal strength by weighting the branch cross-correlation functions accordingly. All the figures discussed below are plotted at a constant scale to facilitate direct comparison of the results.

RESULTS

In our first two experiments, we examine the resolving power of a single source recorded at a single receiver as a function of source depth. Figure 4 presents the resolution and covariance operators for the source at 119 km depth. These operators are plotted as a function of two depth variables, with the vertical axis identified as 'target depth.' Each row of \mathbf{R}_m may be characterized as the resolving kernel for a specific target depth. For example, the kernel at 150 km depth ideally should be a delta function centered at 150 km. Although it is peaked, this particular kernel has a width of approximately 200 km, which indicates that the model-perturbation estimate at 150 km depth is a weighted average of the true model perturbation from about 50 to 250 km. The absence of sidelobes signifies that the averaging is localized. The amplitude of the resolving kernels in this experiment falls off rapidly with depth and is essentially flat by 300 km, restricting resolution to the top of the upper mantle. The covariance operator describes how errors in the data map into errors in the model perturbation estimate. The diagonal elements of \mathbf{V}_m represent the marginal variance of the model values, while the off-diagonal terms measure the correlation between errors at one depth with errors at other depths. In this experiment, the variance is pronounced at shallow depths, with high amplitudes in the diagonal and off-diagonal elements, but decreases with depth. The variance is low where the resolving kernel amplitude is small and higher at shallow depths where the kernel amplitude is large, which is a manifestation of the trade-off between bias and covariance.

Figure 5 depicts the same experiment for a single deep source ($h=552$ km). In contrast to Figure 4, the resolving kernels are peaked down to target depths as great as 600 km. These kernels

are generally narrower than those for the shallow source, although the width increases with depth. Unlike the kernels in Figure 4, however, these have well-developed sidebands, which indicate that the averaging is not localized. The overall increase in resolution at depth is mirrored by an increase in the variance. The covariance operator for this experiment has high-amplitude diagonal terms and considerable structure in the off-diagonal elements.

Comparison of Figures 4 and 5 illustrates the contribution of higher-mode data to resolution of upper-mantle structure. It is clear from Figure 1 that the seismogram for the shallow source is dominated by the fundamental mode, with very little excitation of the higher modes. With the branch cross-correlation functions all weighted equally, the fundamental mode controls the inversion, restricting resolution to depths shallower than 200 km. On the other hand, the seismogram for the source at 552 km depth contains very little fundamental-mode information; the inversion is controlled primarily by the second, third, and fourth higher modes. Higher-mode dispersion is more sensitive to structures at depth than fundamental-mode dispersion, and this is reflected in the resolution operator of Figure 5.

In the next two experiments, we examine the effect of expanding the number of receivers from one to five. Figure 6 presents the results from the experiment with the deep source recorded at the array of receivers. The resolution operator for this experiment is smoother and the peaks are narrower with higher amplitudes than the kernels in Figure 5. This increase in resolution is not surprising, as the array spans the triplication of *SSS*, a phase which bottoms between 400 and 800 km. Since *SSS* samples the lower part of the upper mantle, the triplication provides valuable information about the structure at these depths. However, the greatest gain from the expansion of the receiver array is observed in the covariance operator. The array reduces the variance of the solution by nearly a factor of five, since we assumed that the errors in the differential branch cross-correlation functions are uncorrelated. Figure 7 displays the resolution and covariance operators for the experiment with the shallow source and the array of receivers. Comparison of Figures 7 and 4 shows that only a marginal improvement in resolution results in this case, although the amplitude of the covariance operator is decreased by nearly a factor of five.

Although the primary benefit from an array of receivers appears to be the reduction of the covariance operator, we can take advantage of the relationship between resolution and covariance (which is governed by the parameters α and β in equation 19) to exchange some of the decrease in covariance for an increase in resolution. Figure 8 shows the results from increasing α and decreasing β in a fixed ratio for the experiment with the deep source recorded at the array of receivers. Although the resolving kernels are narrower and more peaked for this translation along the trade-off curve, the cost in terms of the reliability of the solution is quite high. The covariance operator for this experiment is not well behaved, with errors at one depth scaling with errors at nearly all depths. Figure 9 presents the results for a translation along the trade-off curve in the other direction. In this case, the resolution operator is highly degraded, while the covariance operator is nearly flat. We can also experiment with the trade-off parameters for the shallow source recorded at the array of receivers, resolution is limited more by the depth of the source (given the 'natural' weighting of the branch cross-correlation functions) than by the number of receivers in this experiment.

Having examined the dependence of the resolution and covariance operators on an array of receivers, we model the effect of an array of sources. Figure 10 shows the results from an experiment with five sources distributed in depth from 119 to 552 km and recorded at a single station. From a comparison of Figures 4 and 5 with Figure 10, it is clear that a distribution of sources can be particularly effective in enhancing resolution. The resolution kernels of Figure 10 have high-amplitude and narrow peaks and show some resolution as deep as 600-700 km depth. The sideband structure is damped, although the averaging is not completely localized. In terms of the covariance operator, an array of sources reduces the variance considerably, but not as effectively as an array of receivers. Figure 11 illustrates the resolution and covariance operators for the optimal experiment of five sources recorded at five receivers. As before, the addition of five

receivers narrows the peaks of the resolution kernels, but the greatest gain is in the reduction of the variance.

In these six experiments, the branch cross-correlation functions are effectively weighted by their relative amplitudes in the inversion, since the error at zero lag, σ_i , is assumed to be independent of the branch number. This 'natural' weighting entails certain implicit assumptions about the error process. If one assumes that errors in the data are introduced strictly by the presence of ambient seismic noise (wind, microseisms, cultural noise, etc.), then this natural weighting by the relative excitation of the modes is most appropriate. In that case, the highest amplitudes carry the greatest weight since they have the best signal-to-noise ratio. However, many errors may be a function of signal strength (such as multipathing, source structure, etc.). If these errors dominate the random processes, then the natural weighting is not appropriate.

We explore the effect of characterizing the error processes by experimenting with the mode branch weights for the shallow source recorded at one and five receivers. By increasing the weight of the higher-mode branches relative to the fundamental, we model the case where the errors scale with signal strength. Figure 12 illustrates the resolution and covariance operators for this experiment. Comparing Figures 4 and 12, it is clear that this weighting of the higher-mode signals has improved the resolution at depth, although these kernels are neither narrow nor localized. The increase in resolution is reflected by an increase in the variance. As before, increasing the number of receivers (Figure 13) marginally improves the resolution, but dramatically decreases the variance of the solution. The results from these two experiments highlight the importance of the assumptions made about the error process. If errors scale with signal strength (which we think is more realistic), then the branch cross-correlation functions need to be weighted accordingly. However, the weighting of the branch cross-correlation functions plays an important role in the resolving power of a particular experiment, as it is possible to obtain some resolution at depth even from a shallow source when the contributions from the higher-mode branches are weighted appropriately.

CONCLUSIONS

In this study, we augment the waveform inversion technique of *Lerner-Lam and Jordan* [1983] with a resolving power analysis and use this capability to examine some issues in experimental design. These experiments have demonstrated several important results. First, fundamental-mode data alone cannot resolve structure at depths greater than 200 km; a fact which has been appreciated by seismologists for many years. Higher-mode information, which samples greater depths, is essential to obtain resolution of the upper mantle. Second, a single station is capable of nearly the same resolving power as a dense array of receivers with this method, since the higher-mode waveform inversion technique does not rely on spatial transforms. The advantage of such an array comes primarily through the reduction of the variance of the solution, although the decrease in covariance may be exchanged for an increase in resolution through the trade-off parameters. Third, source arrays are particularly effective in enhancing resolution at depth, provided that the source depths are well distributed and the source centroids and moment tensors are well determined. Finally, the characterization of the error processes plays an important role in the resolving power analysis of a particular experiment, since the relative weighting of the branch cross-correlation functions will influence the resolution. Since the waveform inversion technique permits the contribution of each branch cross-correlation function to be assessed and weighted separately, resolution of structure at depth is possible even with shallow sources.

REFERENCES

- Backus, G.E., and J.F. Gilbert, Uniqueness in the inversion of inaccurate gross Earth data, *Phil. Trans. R. Soc. A.*, **266**, 123-192, 1970.
- Cara, M., Regional variations of higher Rayleigh-mode velocities: a spatial filtering method, *Geophys. J. R. astr. Soc.*, **54**, 439-460, 1978.
- Cara, M., Lateral variations of S velocity in the upper mantle from higher Rayleigh modes, *Geophys. J. R. astr. Soc.*, **57**, 649-670, 1979.
- Cara, M., A. Nercessian, and G. Nolet, New inferences from higher mode data in western Europe and northern Eurasia, *Geophys. J. R. astr. Soc.*, **61**, 459-478, 1980.
- Chou, T., and A. Dziewonski, Regional variations in the structure of upper mantle from dispersion of overtones of surface waves, unpublished manuscript, 1980.
- Davies, G.F., Thickness and thermal history of continental crust and root zones, *Earth Planet. Sci. Lett.*, **44**, 231-238, 1979.
- Dost, B., A.V. Wettum, and G. Nolet, The NARS array, *Geol. Mijnbouw*, **63**, 381-386, 1984.
- Dziewonski, A.M., T.-A. Chou, and J. Woodhouse, Determination of earthquake source parameters from waveform data for studies of global and regional seismicity, *J. Geophys. Res.*, **86**, 2825-2852, 1981.
- Dziewonski, A.M., J.E. Franzen, and J.H. Woodhouse, Centroid-moment tensor solutions for January-March, 1984, *Phys. Earth Planet. Int.*, **34**, 209-209, 1984.
- Dziewonski, A.M., A. Friedman, and J.H. Woodhouse, Global seismicity of 1982: centroid-moment tensor solutions for 308 earthquakes, *Phys. Earth Planet. Int.*, **33**, 76-90, 1983.
- Feng, C. and Teng T., Three-dimensional crust and upper mantle structure of the Eurasian continent, *J. Geophys. Res.*, **88**, 2261-2272, 1983.
- Gilbert, F., The representation of seismic displacements in terms of travelling waves, *Geophys. J. R. astr. Soc.*, **44**, 275-280, 1976.
- Grand, S.P. and D.V. Helmberger, Upper mantle shear structure of North America, *Geophys. J. R. astr. Soc.*, **76**, 399-438, 1984a.
- Grand, S.P. and D.V. Helmberger, Upper mantle shear structure beneath the northwestern Atlantic Ocean, *J. Geophys. Res.*, **89**, 11465-11475, 1984b.
- Grand, S.P., D.V. Helmberger, and L.J. Burdick, Attenuation bias measurements of the Semipalatinsk and North African test sites from multiple S phases, *Report WCCP-R-85-01*, Woodward-Clyde Consultants, Pasadena, 27pp, 1985.
- Jordan, T.H., The continental tectosphere, *Rev. Geophys. Space Phys.*, **13**, 1-12, 1975.
- Jordan, T.H., Composition and development of the continental tectosphere, *Nature*, **274**, 544-548, 1978.
- Jordan, T.H., Continents as a chemical boundary layer, *Phil. Trans. R. Soc. Lond. A.*, **301**, 359-373, 1981.
- Lerner-Lam, A.L., Linearized estimation of higher-mode surface wave dispersion, *Ph.D thesis*, University of California, San Diego, 1982.

- Lerner-Lam, A.L. and T.H. Jordan, Earth structure from fundamental and higher-mode waveform analysis, *Geophys. J. R. astr. Soc.*, **75**, 759-797, 1983
- Masters, G. and F. Gilbert, Attenuation in the earth at low frequencies, *Phil. Trans. R. Soc. Lond. A.*, **308**, 479-552, 1983.
- Merete, W., *Geophysical data analysis: discrete inverse theory*, Academic Press Inc., London, 260 p., 1984.
- Nolet, G., Higher Rayleigh modes in western Europe, *Geophys. Res. Lett.*, **2**, 60-62, 1975.
- Nolet, G., Higher modes and the determination of upper mantle structure, *Ph.D thesis*, Utrecht, 1976.
- Nolet, G., Simultaneous inversion of seismic data, *Geophys. J. R. astr. Soc.*, **55**, 679-691, 1978.
- Nolet, G., B. Dost, and H. Paulssen, Intermediate wavelength seismology and the NARS experiment, *Annal. Geophysic.*, (submitted), 1985.
- Richter, F., Models for the Archean thermal regime, *Earth Planet. Sci. Lett.*, **73**, 350-360, 1985.
- Sipkin, S.A. and T.H. Jordan, Lateral heterogeneity of the upper mantle determined from the travel times of multiple ScS, *J. Geophys. Res.*, **81**, 6307-6320, 1976.
- Wiggins, R.A., The general linear inverse problem: Implication of surface waves and free oscillations for Earth structure, *Rev. Geophys. Space Phys.*, **10**, 251-285, 1972.
- Woodhouse, J. and F. Dahlen, The effect of a general aspherical perturbation on the free oscillations of the Earth, *Geophys. J. R. astr. Soc.*, **53**, 335-354, 1978.

Table 1
The Receiver Array

Station I.D.	Latitude (°)	Longitude (°)
KONO01	59.648	9.597
KONO05	62.318	15.746
KONO09	64.665	23.013
KONO13	66.592	31.520
KONO17	67.989	41.243

Table 2
The Source Array

Date	Latitude(°)	Longitude (°)	Depth (km)	Magnitude
07/04/82	27.92	136.48	551.8	6.3
07/05/82	30.77	130.47	119.0	5.7
09/06/82	29.18	140.65	155.6	6.6
01/01/84	33.38	136.81	383.6	6.5
02/13/84	25.26	122.29	268.2	5.5

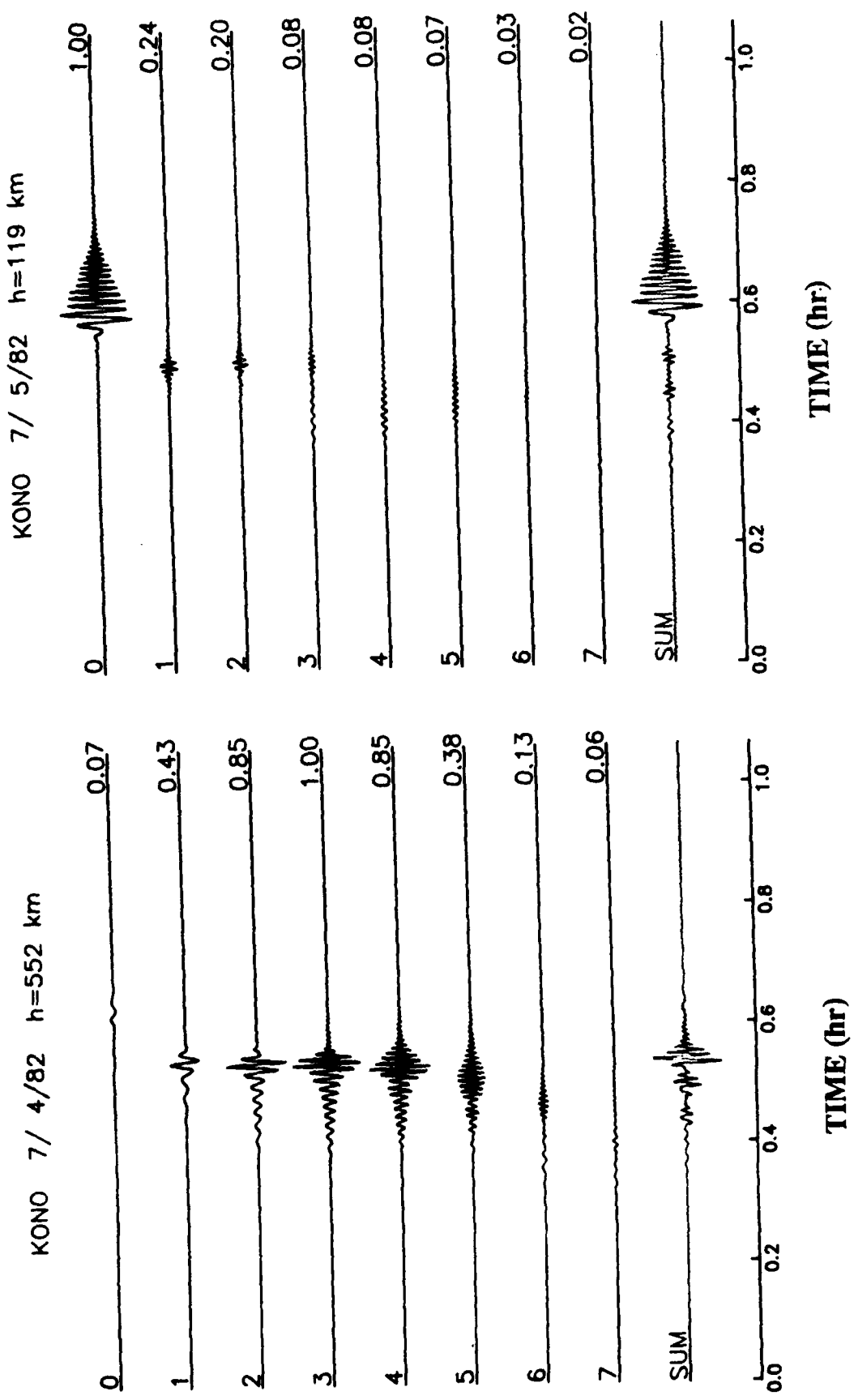


Figure 1: The fundamental and first seven overtone mode-branch synthetics are plotted for events 07/04/82 ($h=552$ km) and 07/05/82 ($h=119$ km) at the station KONNO01. The numbers on the right of each plot indicate the relative excitation of the various modes, normalized to the highest amplitude. This figure demonstrates the excitation of the modes as a function of depth. The fundamental mode dominates the arrivals in the shallow event, while the higher modes eclipse the fundamental mode in the deeper event.

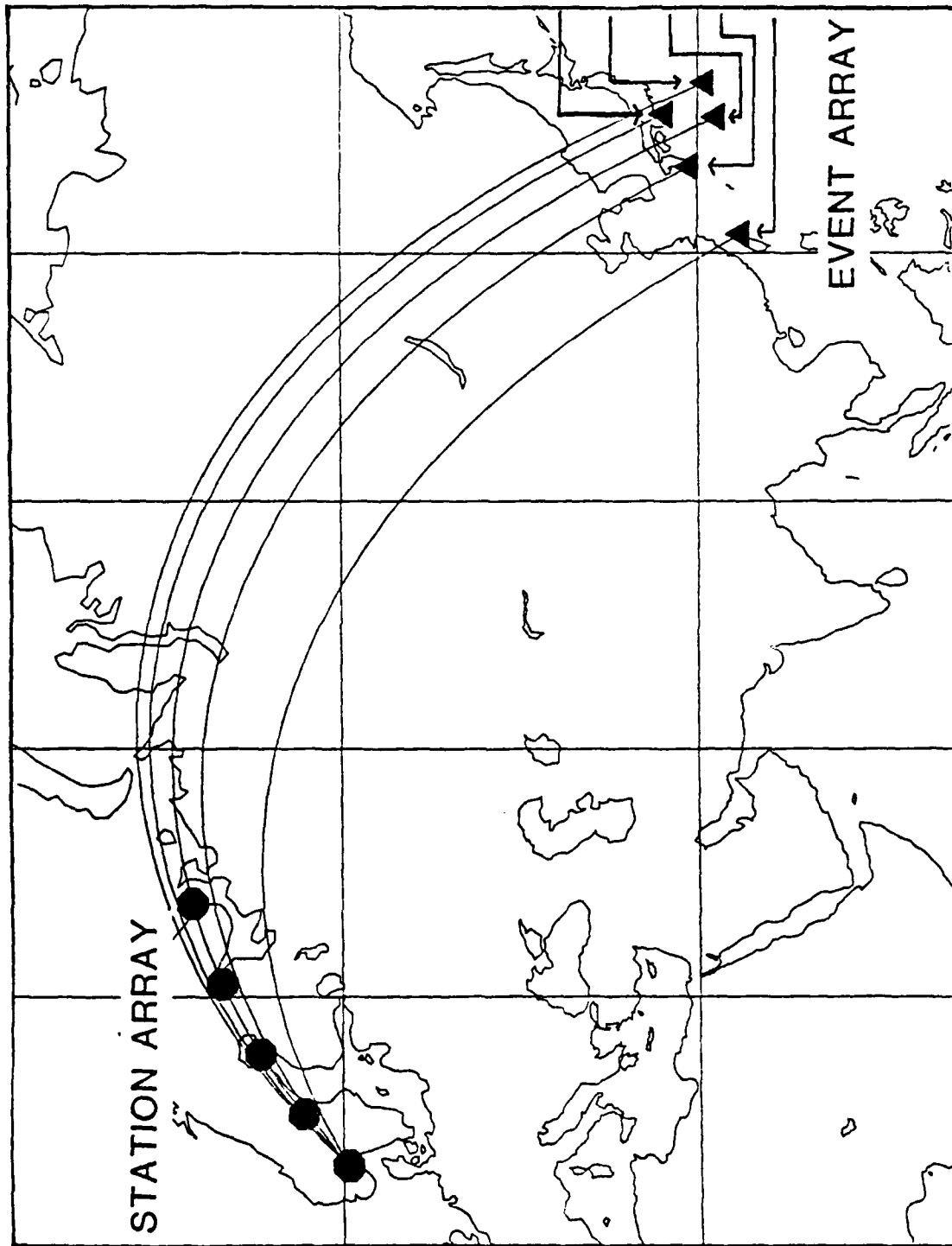


Figure 2: This map shows the configuration of the sources and receivers used in this study. The source array is a cluster of five earthquakes located south of Japan, with source depths ranging from 119 to 552 km. The receiver array is modelled after the NARS array, and spans an aperture of 16° with 4° spacing between stations.

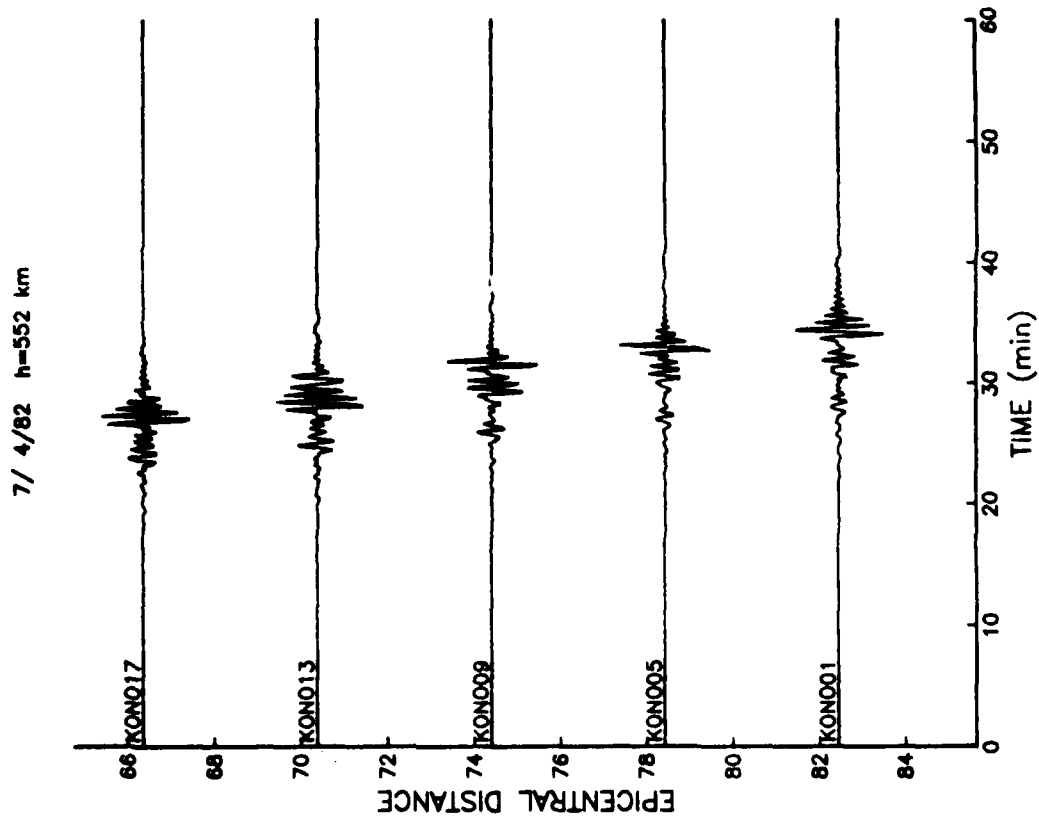
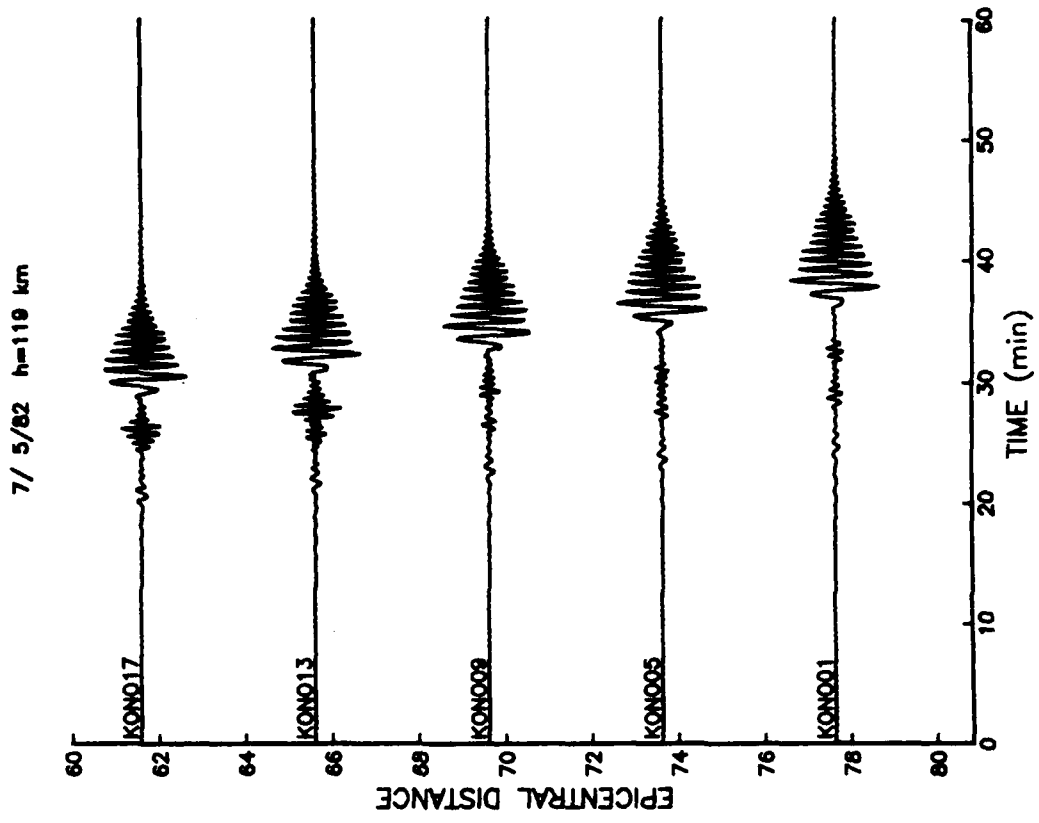


Figure 3: This figure illustrates the synthetic seismograms calculated for the receiver array for the events 07/04/82 and 07/05/82. The stations span the triplication of SSS, which provides critical information about the lower part of the upper mantle.

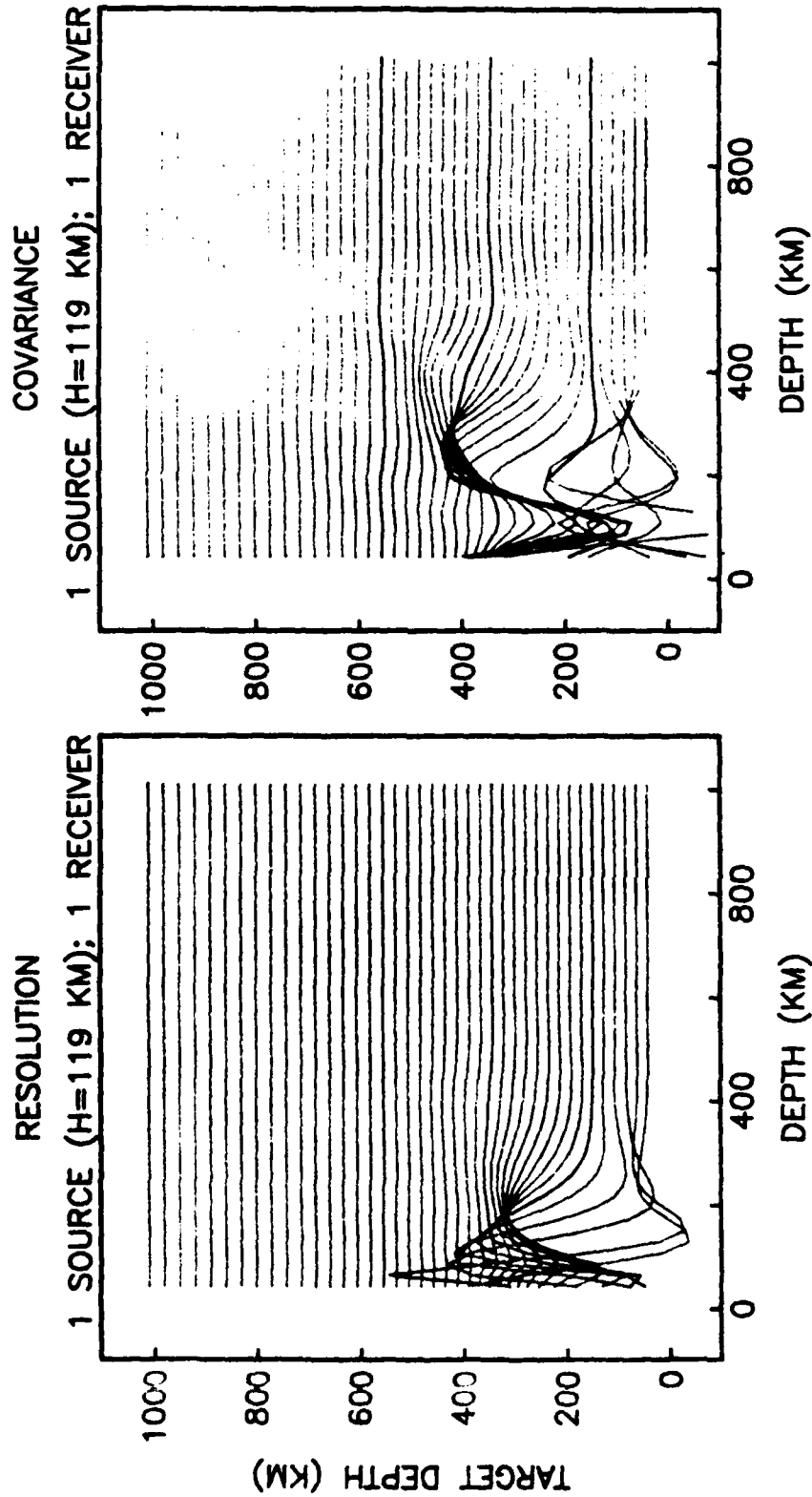


Figure 4: The resolution and covariance operators for the experiment of a shallow source ($h=119$ km) recorded at a single receiver are presented in this figure, with target depth plotted as a function of depth. The resolving kernels are peaked at shallow depths in this experiment, which reflects the excitation of the fundamental mode. The variance of the solution is high at shallow depths, but decreases rapidly. In the following figures, the resolution and covariance operators have been scaled so that the results of one experiment may be compared with another.

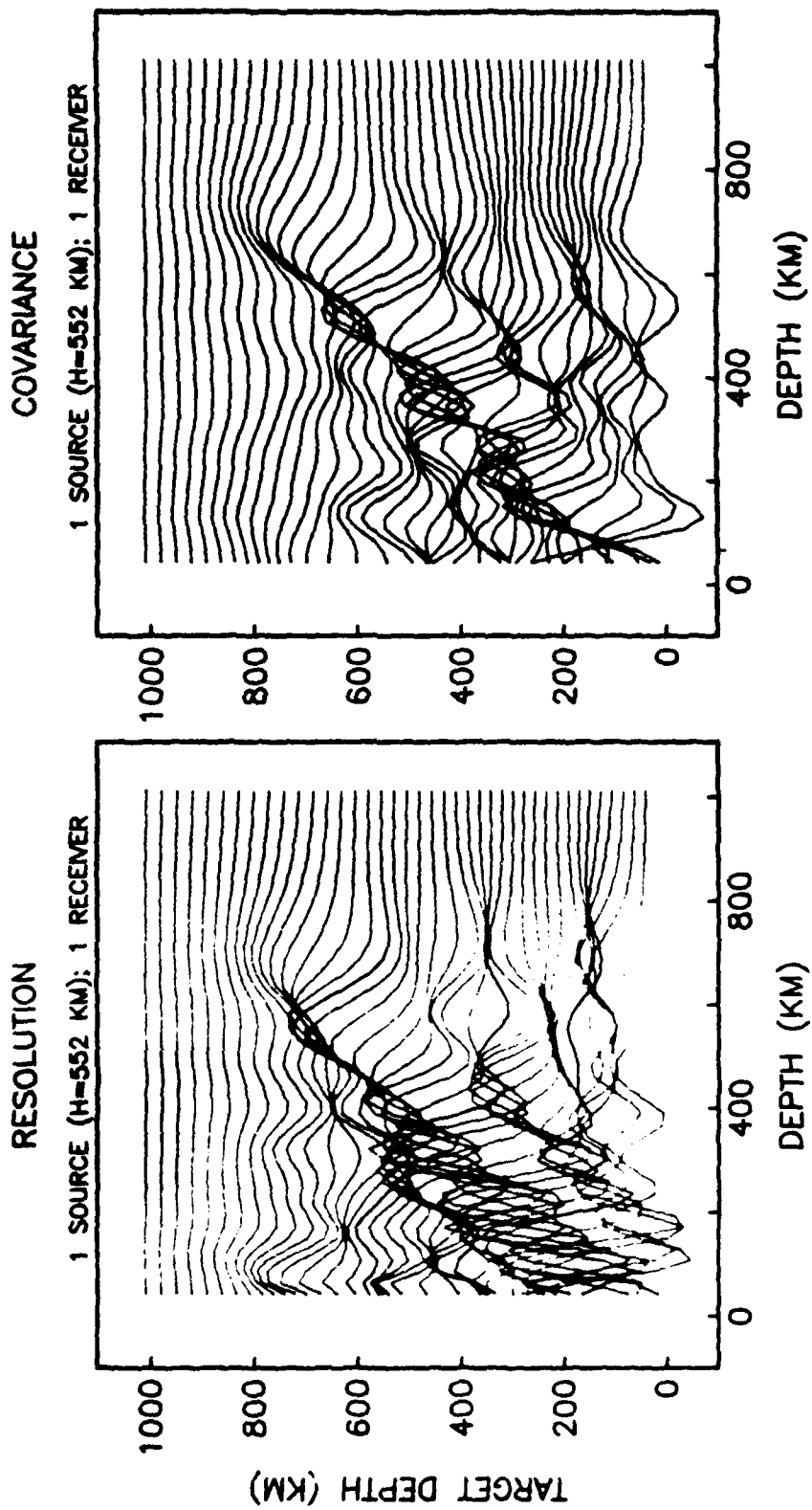


Figure 5: This figure shows the resolution and covariance operators for a deep source ($h=552$ km) recorded at a single receiver. Comparison with Figure 6 demonstrates how the addition of higher-mode information improves the resolution of upper-mantle structure. In this experiment, the fundamental mode is not excited, and the higher modes dominate the seismogram. Consequently, the resolving kernels are peaked down to 600 km, although the peaks are not well localized.

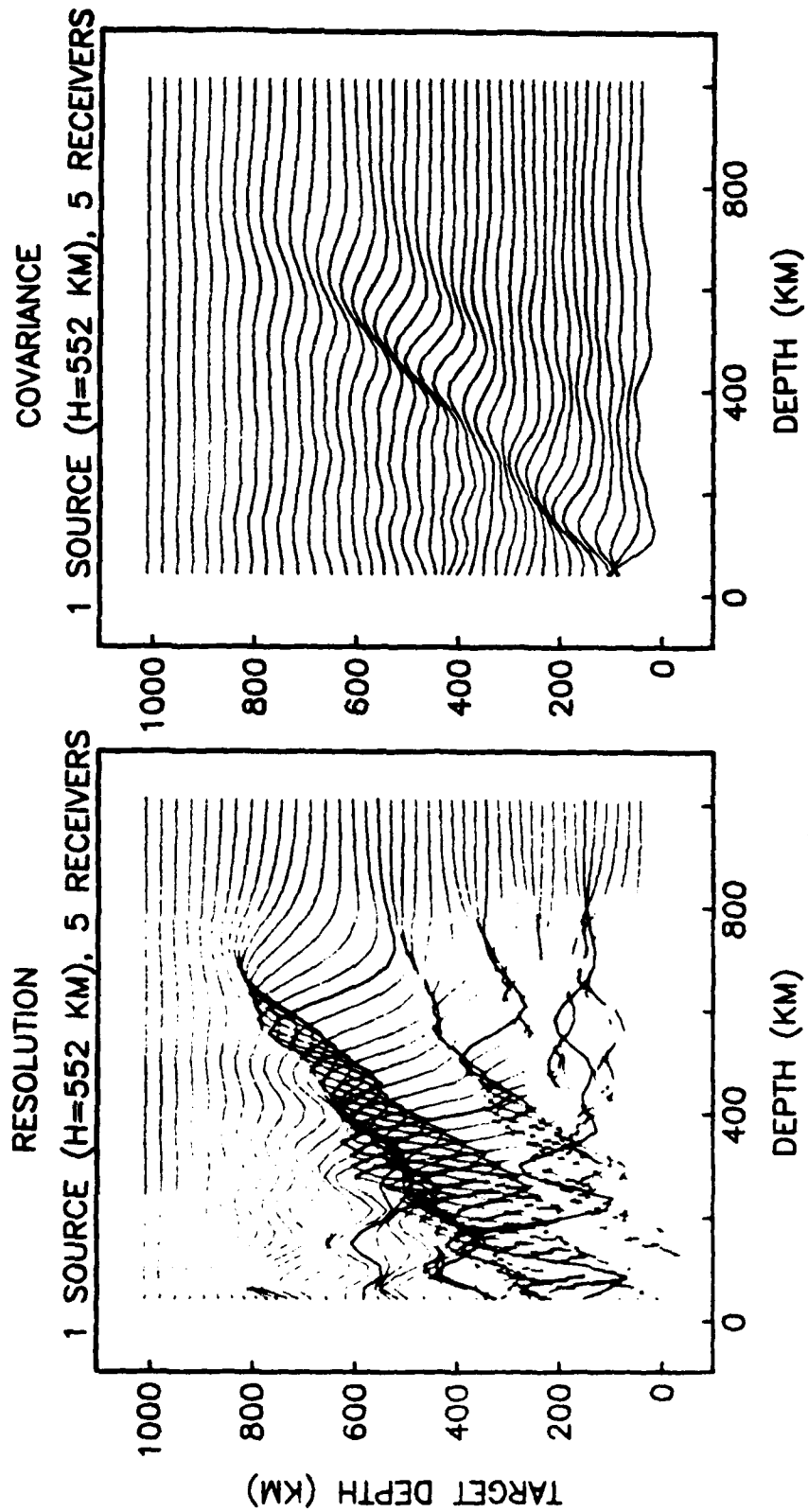


Figure 6: This figure displays the resolution and covariance operators for a deep source recorded at the array of receivers. The resolving kernels have been smoothed and their peaks narrowed in this experiment, while the covariance has come down by a nearly a factor of five.

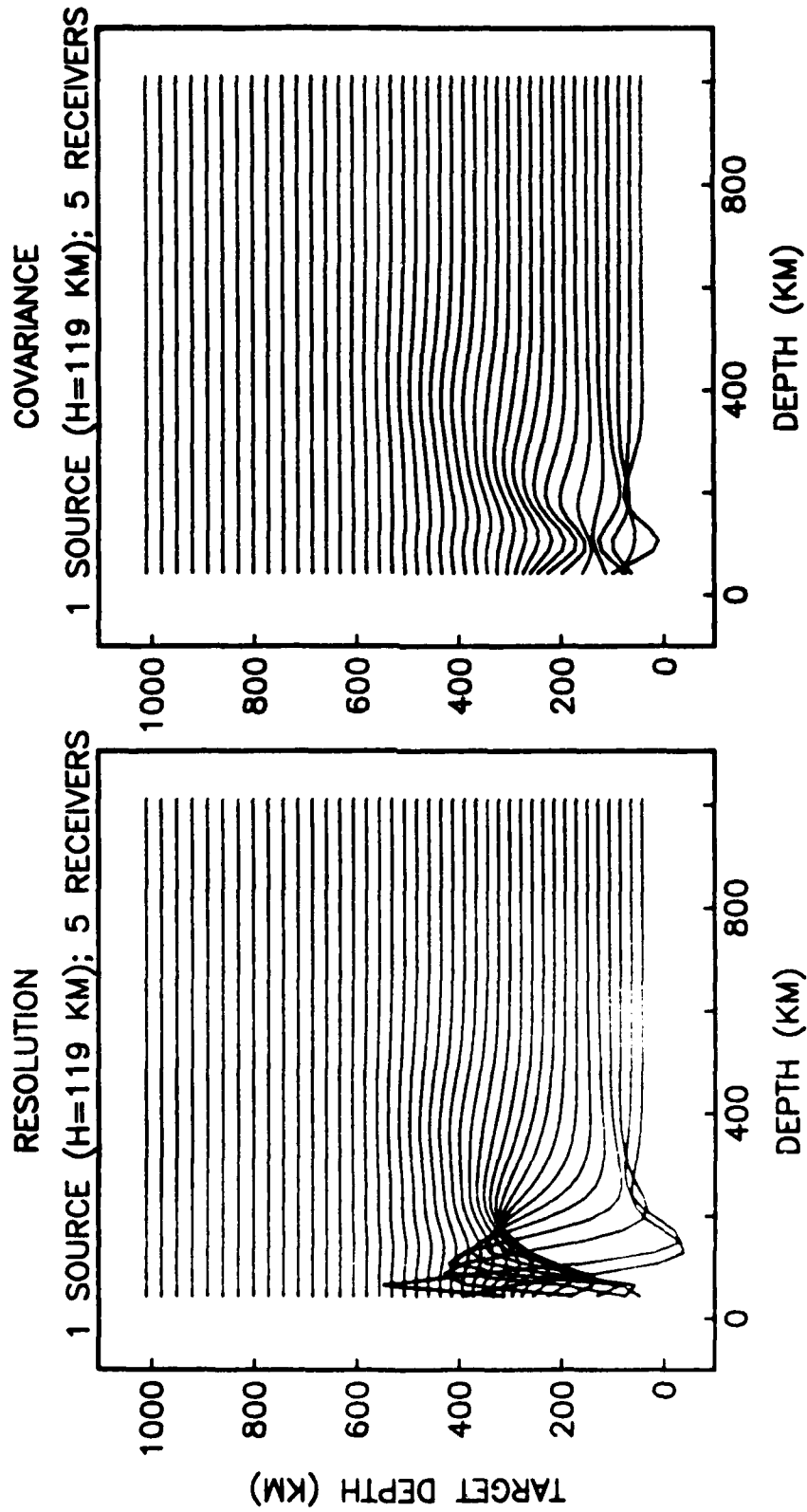


Figure 7: The resolution and covariance operators for the shallow event recorded at five receivers are plotted in this figure. For constant values of α and β , the addition of a receiver array results in marginal improvement in the resolution, although the covariance is cut down by nearly a factor of five. In this experiment, the resolving power is constrained more by the depth of the source than by the number of receivers.

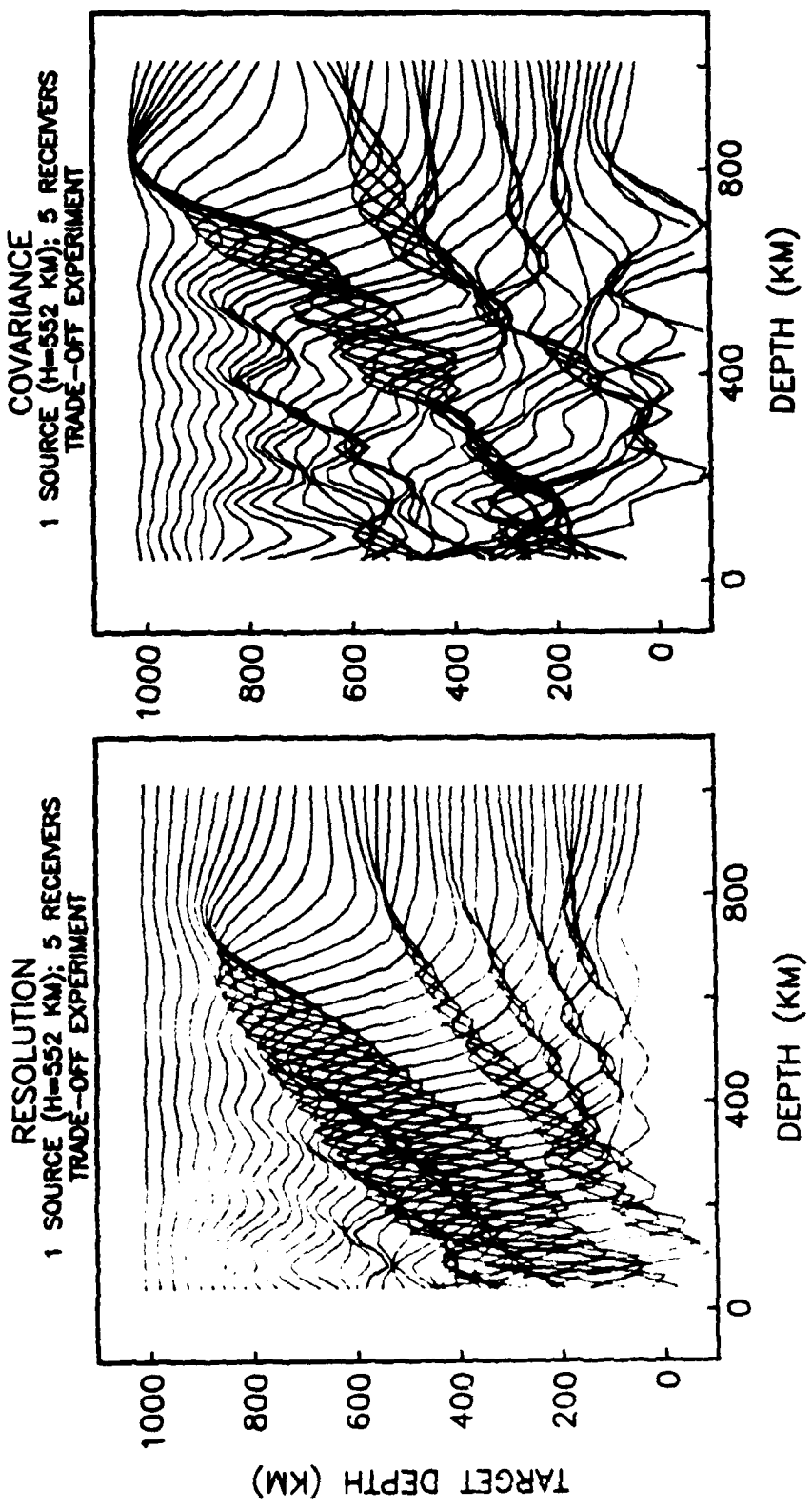


Figure 8: Since the receiver array has reduced the covariance so dramatically, it is possible to experiment with the trade-off curve and exchange the reduction in covariance for an increase in resolution. Figure 8 demonstrates the results from an inversion where α and β were varied in a fixed ratio. Comparing Figures 6 and 8, it is clear that the resolution can be improved, although the cost in terms of the increase in the covariance is quite high.

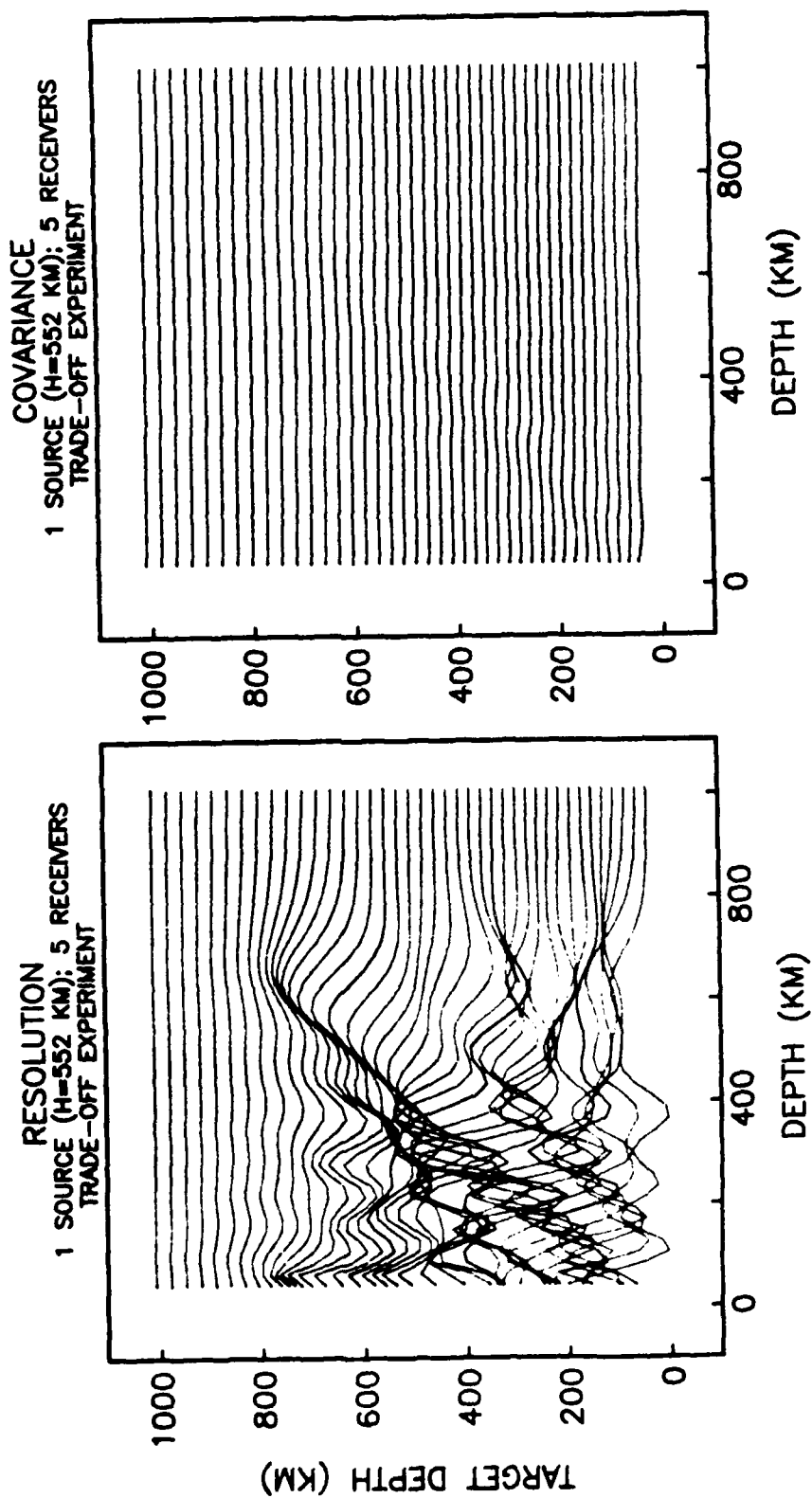


Figure 9: Figure 9 shows the result from moving in the other direction on the trade-off curve. In this case, the covariance is nearly flat, but the resolving kernels have been severely degraded.

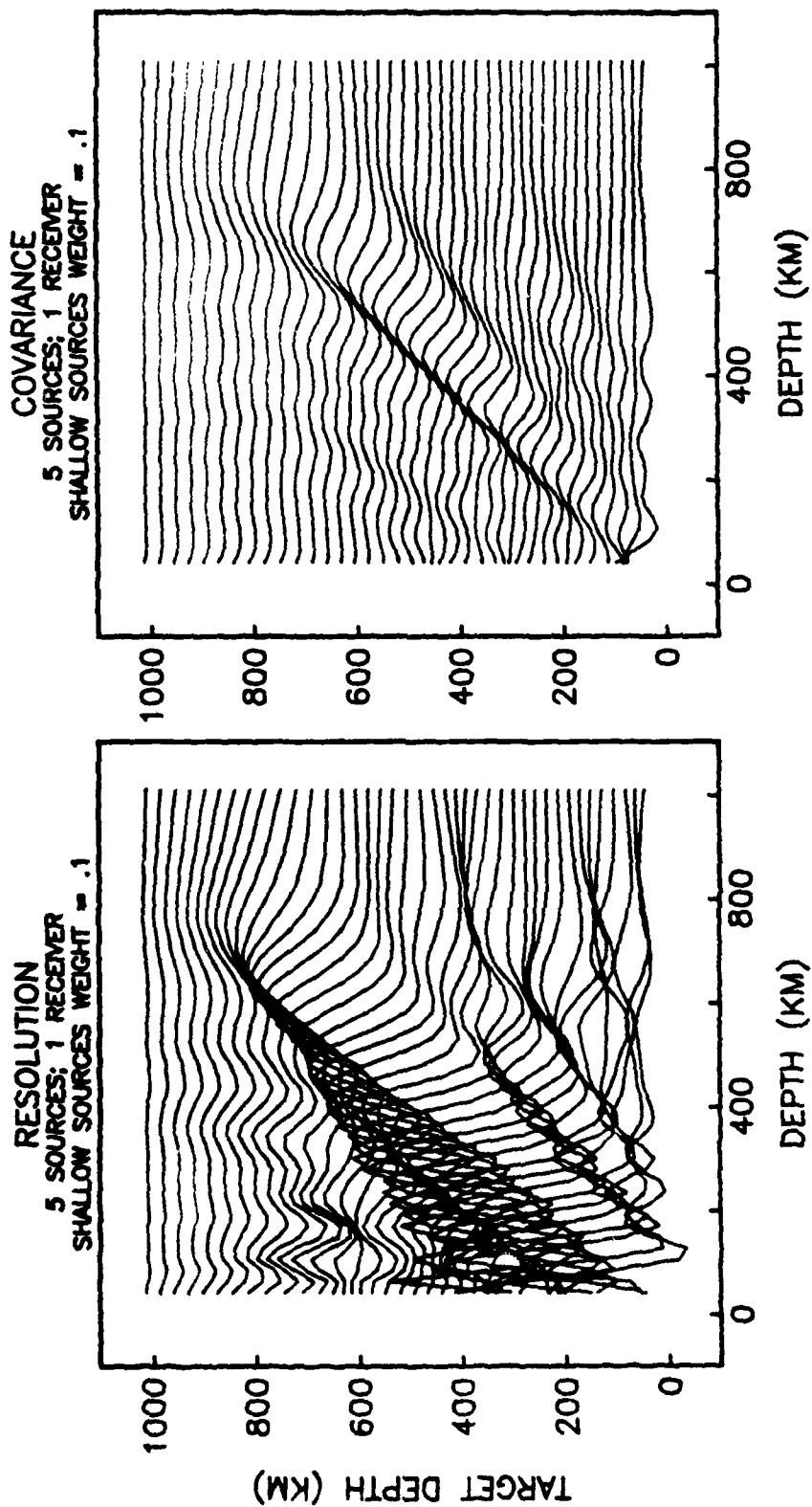


Figure 10: The resolution and covariance operators are displayed for the experiment with five sources recorded at a single receiver. The addition of a source array distributed in depth improves the resolving power considerably. In this experiment, the amplitude of the resolving kernels is peaked and quite narrow, with damped sideband structure, while the covariance is low. The addition of the higher modes, which sample a range of phase velocities, provides critical information for the resolution of upper-mantle structure.

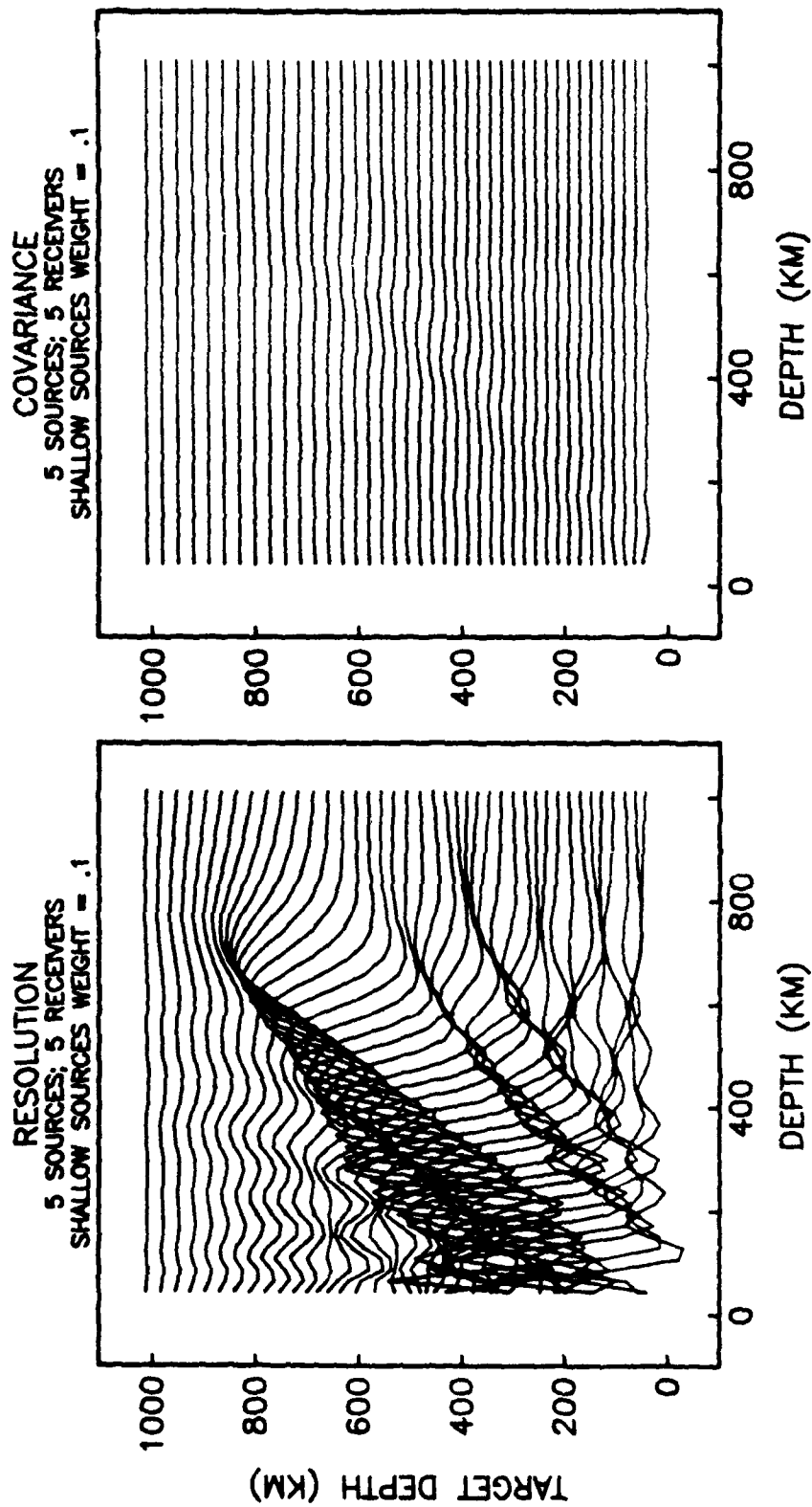
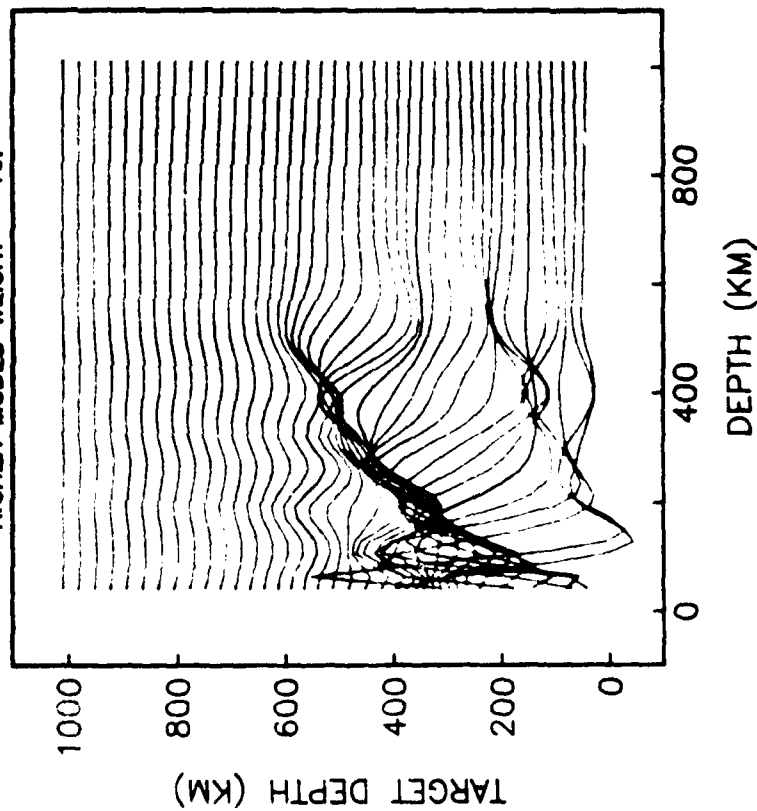


Figure 11: This figure presents the resolution and covariance operators for the optimal experiment of five sources recorded at five receivers. As before, the addition of the receiver array has smoothed the resolving kernels and narrowed the peaks, while damping the covariance. Similar to experiment of Figure 8, this reduction in the covariance may be traded for an increase in resolution.

RESOLUTION
1 SOURCE (H=119 KM); 1 RECEIVER
HIGHER MODES WEIGHT = 10.



COVARIANCE
1 SOURCE (H=119 KM); 1 RECEIVER
HIGHER MODES WEIGHT = 10.

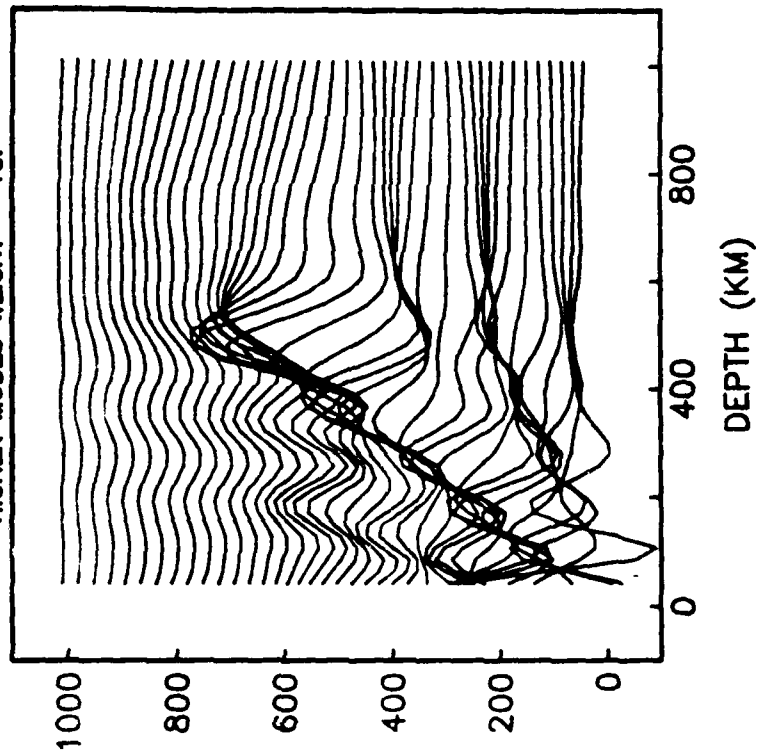


Figure 12: This experiment with the shallow source and a single receiver assumes a noise model where errors scale with signal strength. Consequently, the higher mode branches were given higher weight in the inversion relative to the fundamental mode branch. As a result of the upweighting of the higher modes, the resolution at depth has improved.

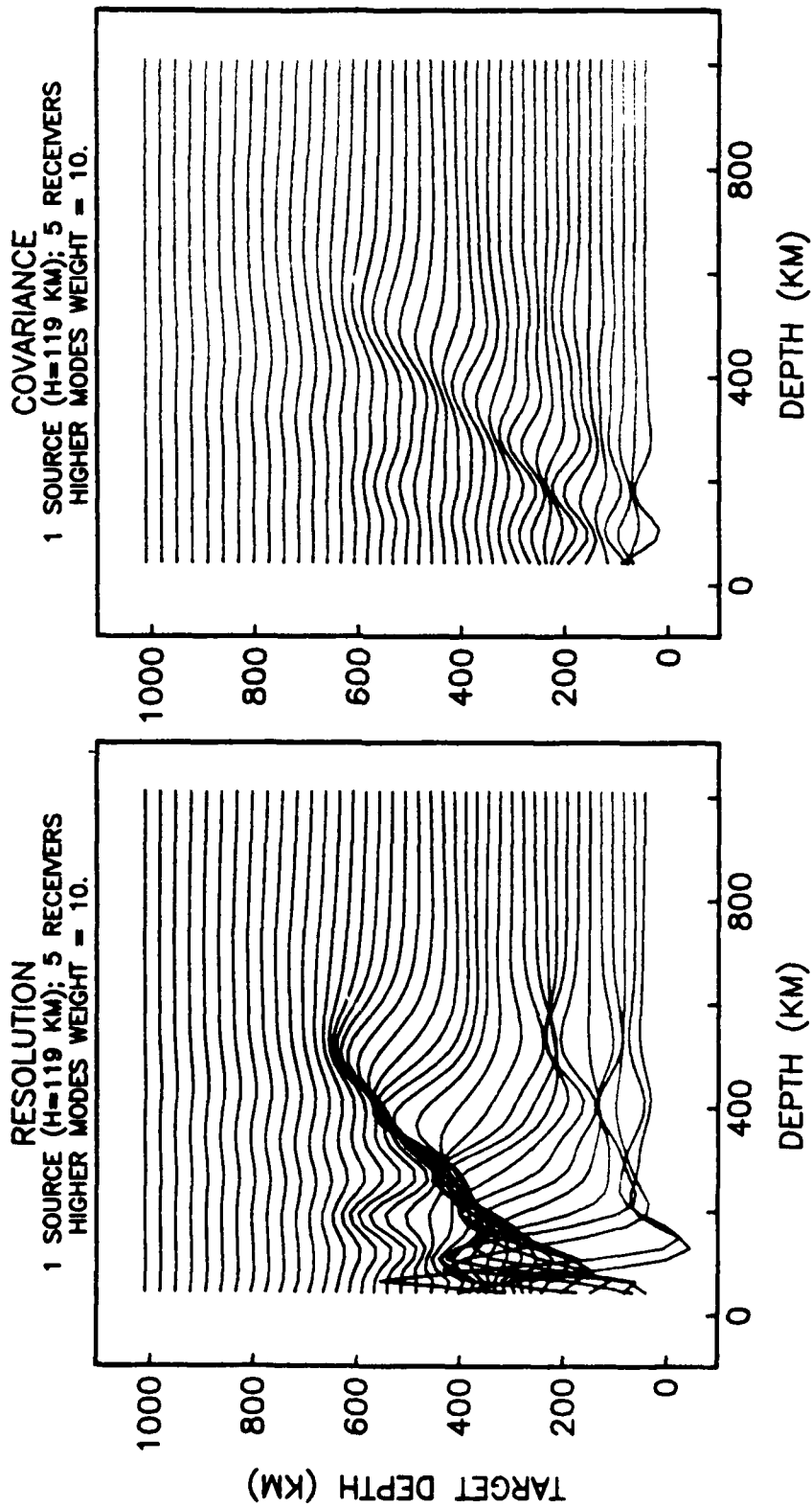


Figure 13: This figure expands the noise model experiment to the shallow source recorded at five receivers. As before, the addition of the receiver array gives a reduction in covariance which may be traded-off for an improvement in resolution.

DTIC

FILMED

4-86

END